A Numerical and Experimental Approach to study the Parametric Effect of Ultrasonic Welding

A Thesis Submitted
In Partial Fulfillment of the Requirements
For the Award

of

Master of Technology
(Production Engineering)

by

Manas Ranjan Panda
Roll No. 213ME2414

Under the supervision of
Prof. S. S. Mahapatra

National Institute of Technology, Rourkela
राष्ट्रीय प्रौद्योगिकी संस्थान, राउरकेला
Odisha (India)-769008
MAY 2015

Declaration

I do, hereby, declare that this submission is my own work and that, to the best of my knowledge and belief, it contains no material previously published or written by another person nor material which to a substantial extent has been accepted for the award of any other degree or diploma of the university or other institute of higher learning, except where due acknowledgement has been made in the text.

Place: NIT Rourkela *Manas Ranjan Panda*
Date:

NATIONAL INSTITUTE OF TECHNOLOGY, ROURKELA -769008, ODISHA, INDIA

Certificate

This to certify that the thesis entitled - **A Numerical and Experimental Approach to study the Parametric Effect of Ultrasonic Welding** being submitted by **Manas Ranjan Panda** for the award of the degree of Master of Technology (Mechanical Engineering) of NIT Rourkela, is a record of bonafide research work carried out by him under our supervision and guidance. **Manas Ranjan Panda** has worked for more than two years on the above problem at the Department of Mechanical Engineering, National Institute of Technology, Rourkela and this has reached the standard fulfilling the requirements and the regulation relating to the degree. The contents of this thesis, in full or part, have not been submitted to any other university or institution for the award of any degree or diploma.

Prof. Siba Sankar Mahapatra
(Supervisor)
Department of Mechanical Engineering
National Institute of Technology
Rourkela-769008, Odisha, India

Dedicated to

My guide

Parents

And

Friends

ACKNOWLEDGEMENTS

Foremost, I would like to express my heartfelt gratitude and warm regards to **Prof. S. S. Mahapatra**, my research supervisor and Head of the Department, for his patience, continuous support, encouragement, timely guidance, discussions and suggestions. His guidance, great moral support and inspiration helped me throughout the journey of my research and the improvement of writing the thesis. I consider myself fortunate to have had the opportunity to work under his able guidance and enrich myself from his depth of knowledge.

Besides my supervisor, I would like to thank to **Prof. Sunil Kumar Sarangi**, Director of National Institute of Technology, Rourkela, **Prof. S. K. Sahoo** and **Prof. S Datta** of Mechanical Engineering Department for their kind support and concern regarding my academic requirement. Also, specia1 thanks to all my teachers of Mechanical Engineering Department of National Institute of Technology, Rourkela for the knowledge they offered.

No words are sufficient to express my heartfelt gratitude to beloved Mr. Suman Chatterjee, Mr. Chinmay Mohanty, Mr. Kumar Abhishek, Mr. Mantra Prasad Satpathy, Mr. Swayam Bikas Misra, Mr. Chitrasen Samantra, Mrs. Bijaya Bijeta Nayak, Ms. Sanjita Jaipuria, Mr. Dilip Sen, Mr. Amit Meher and Mrs. Shrutee Nigam research scholar, for the rock solid support they have rendered at the time of adversity during my research work and preparation of the thesis.

Last but not the least; I thank the one above all of us, the omnipresent God, for giving me the strength during the course of this research work.

Manas Ranjan Panda

ABSTRACT

In today's world, aluminium and its alloy is showing promising characteristics for replacing other materials due its excellent properties like light weight, corrosion resistance, high strength and toughness. Conventional welding for these materials creates some challenges like porosity, hot cracking and void formation. Ultrasonic welding gives some ultimate solution to these problems as the material experience only 30% of its melting point temperature. Ultrasonic welding is a creative system for joining metals and composites rapidly and safely owing to a high-frequency vibration consolidated with pressure. The process has a widespread application in electrical, automotive, aerospace, medical and packaging industry. In the present research work, a numerical model is proposed for the evaluation of heat generation due to deformation and friction during welding. The developed model is equipped for predicting the interface temperature and stress distribution during ultrasonic welding and their impacts on sonotrode, anvil and welded parts. The effect of tool (sonotrode) shape also studied. Response surface methodology (RSM) with Box-Behnken design has been implemented to design the experimental setup and establish a co-relation between process parameters viz. pressure, amplitude and welding time with the output response as tensile strength. RSM is coupled with desirability function is utilized to optimize the parameters for a desired tensile strength of the joint. The result of numerical model is compared with the experimental value and found to be in good agreement.

Keywords: *Ultrasonic welding; FEM; RSM; Desirability function; thermocouple.*

CONTENTS

Declaration ..... **i**

Certificate ..... **ii**

Area of Research Certificate ..... **iii**

Acknowledgements ..... **iv**

Abstract ..... **v**

Contents ..... **vi**

List of Tables ..... **x**

List of Figures ..... **xi**

Nomenclature ..... **xii**

Chapter No.	Title	Page No.
Chapter 1	Background and Motivation	1
	1.1 Introduction	2
	1.2 Fundamental principle	3
	1.2.1 Wedge-reed system	5
	1.2.2 Lateral-drive system	5
	1.3 Summary	6
Chapter 2	Literature Survey	7
	2.1 On FE Analysis of USW	8
	2.2 On Sonotrode Design of USW	9
	2.3 On Optimization of USW	10
	2.4 Research Objective	13
Chapter 3	Mechanics of Ultrasonic Welding	14
	3.1 Shear force acting on the sonotrode tip	15
	3.2 Contact stress at interface	17
	3.3 Shear forces at weld interface	17
	3.4 Forces at weld interface	19
	3.5 Heat generation during welding	21
	3.5.1 Heat generation at the weld interface due to deformation	22
	3.5.2 Heat generation at the weld interface due to friction	24

	3.6 Summary	25
Chapter 4	Finite Element Modeling: Ultrasonic Welding	26
	4.1 Assumption for the FE model	27
	4.2 Modeling the temperature distribution	27
	4.2.1 Heat flux due to deformation	28
	4.2.2 Heat flux due to friction	29
	4.3 Simulation of the FE model	30
	4.3.1 Boundary conditions	31
	4.3.2 Transient thermal analysis	31
	4.3.3 Transient stress analysis	32
	4.4 Result and discussion	33
	4.4.1 Temperature distribution in the model	33
	4.4.2 Stress distribution in the model	39
	4.5 Summary	42
Chapter 5	Experimentation and Optimization technique	43
	5.1 Response surface methodology	44
	5.1.1 Experimental procedure	45
	5.1.2 Result and discussion	48
	5.2 Optimization using Desirability function	53
	5.3 Validating the FE model for temperature distribution	56
	5.4 Summary	59

Chapter 6	Conclusions	60
	6.1 Summary of the Findings	61
	6.2 Recommendation and Future scope	62
	References	63
	List of Publications	65

LIST OF TABLES

Table No.	Caption	Page No.
Table 4.1	Thermal and Physical properties for workpiece, sonotrode, and anvil	28
Table 4.3	Temperature and stress distribution from the numerical model	42
Table 5.1	Factors with levels	45
Table 5.2	Experimental table	46
Table 5.3	ANOVA for Tensile strength	49
Table 5.4	Desirability Table	55
Table 5.5	Temperature readings with time from lab view software	58

LIST OF FIGURES

Figure No.	Caption	Page No.
Fig. 1.1	Principle of ultrasonic metal welding	4
Fig. 1.2	Types of ultrasonic metal welding system	6
Fig. 3.1	Force morphology of the Wedge-reed System	15
Fig. 4.1	Yield strength variation with respect to temperature	29
Fig. 4.2	Axisymmetry model with boundary conditions	30
Fig. 4.3	Elementary view of the FE model with applied loads	31
Fig. 4.4	Shape and position of nodes for Plane 35 element	32
Fig. 4.5	Temperature distribution with conical shaped sonotrode	34
Fig. 4.6	Temperature distribution with exponential shaped sonotrode	35
Fig. 4.7	Temperature distribution with stepped shaped sonotrode	36
Fig. 4.8	Temperature variation in the workpiece thickness	37
Fig. 4.9	Temperature variation in weld interface along X-direction	38
Fig. 4.10	Temperature variation in the weld interface with each time step	38
Fig. 4.11	Stress distribution with conical shaped sonotrode	39
Fig. 4.12	Stress distribution with exponential shaped sonotrode	40
Fig. 4.13	Stress distribution with exponential shaped sonotrode	41
Fig. 5.1	ASTM Standard (D1002-01) specimen	46
Fig. 5.2	Ultrasonically welded specimens	46
Fig. 5.3	Tested specimens	48
Fig. 5.4	Surface plot of Tensile strength with Amplitude and Pressure	51

Fig. 5.5	Surface plot of tensile strength with Weld time and Pressure	51
Fig. 5.6	Surface plot of tensile strength with Weld time and Amplitude	52
Fig. 5.7	Residual plots for Tensile strength	53
Fig. 5.8	Surface plot for Desirability value with Amplitude and Pressure	56
Fig. 5.9	Experimental set up with temperature measurement attachment	57
Fig. 5.10	Observed temperature variation with time	59

NOMENCLUTURE

A	Area perpendicular to the vibration (mm^2)
A_{DZ}	Area of Deformation Zone (mm^2)
A_{FR}	Area of friction zone (mm^2)
A_S	Area of sonotrode tip (mm^2)
A_{NC}	Non-contact Area (mm^2)
A_W	Weld area (mm^2)
C	Specific heat capacity (J/Kg^0C)
c	Wave Velocity (mm/s)
l	Extension length (mm)
E	Young's modulus (GPa)
F_I	Interface force (N)
F_{FR}	Frictional force (N)
F_N	Clamping force (N)
F_W	Weld force (N)
Fs	Shear force at the sonotrode tip (N)
k	Thermal conductivity (W/m. K)
T	Temperature (^0C)
t	Time (s)
m	Mass of the top part (Kg)
d	Thickness of Material (mm)
Y_T	Temperature dependent yield strength (N/mm^2)

Greek symbols

ρ	Density (Kg/m^3)
γ	Angle of deformation
μ_s	Coefficient of static friction
ξ_0	Sonotrode amplitude (μm)
υ	Poisson's ratio
τ_y	Shear yield stress (MPa)
f	frequency of vibration (Hz)
σ_s	Contact stress (MPa)

CHAPTER 1

BACKGROUND AND MOTIVATION

1.1 Introduction

Ultrasound is the oscillating sound wave having a frequency more than 16 KHz which is well above the human hearing. It can be used for welding of wide range of materials with a frequency more than 20 KHz with vibrational amplitude of more than 10 μm resulting with an ultrasonic energy. Ultrasonic energy is becoming a familiar feature in many industries for different purpose. It harnessed with appreciable benefits for a variety of production applications like plastic welding, ultrasonic cleaning, quality checking and wide advantages in a number of other applications including food processing, automobile, medical, textile industries. Substantial increasing in quality and performance improvements is achieved by using ultrasonic energy in machining technological.

Ultrasonic welding is used for joining two parts by converting electrical energy into heat energy by high frequency mechanical vibrations and is suitable for joining of plastics and metals [1]. This method is effectively used for joining modern engineering structures in automotive and aerospace industries. Ultrasonic welding has great advantages like absence of liquid-solid transformation, low energy consumption, effectively join dissimilar materials and finally, ultrasonic welds are made without consumables such as solder or filler commonly used in conventional joining processes. It is a very fast joining process and does not produce any hazardous gas during welding [2]. There are some restrictions on the types of joints that can be made with ultrasonic welding. It is restricted primarily to the joining of plastics and non-ferrous metals. Another is that, at least one of the parts must be relatively light as it would take tremendous amount of energy to vibrate a heavy part at the necessary frequency. This limitation, unfortunately, restricts the process to small components and wires but owing to the very little welding times, it could be a very economical solution for the joining of mass-produced parts like

clips and brackets in composite based parts of aircrafts and automotive, joining of thin wires, circuit parts in electrical industry.

Ultrasonic welding is a very smart assembling technique for thermoplastic composites. Since it is very fast, hence it does not require any use of external materials, like a metal mesh, at the joint interface irrespective of the behavior of the part being welded and it offers excellent quality joints. Primarily it's focused for the welding of small areas but subsequently it also can be applied for the sequential welding of larger areas [3]. Welding mainly depends upon the joint design where it's needed to concentrate the vibrational energy at the weld interface. The assembly of unreinforced thermoplastic parts is extensively used in the plastics industry but a very few studies has been proposed so far for the assembly of fiber-reinforced thermoplastic composites. So it is been necessary to develop some robust welding procedures by understanding the process parameters is believed to be necessary step towards the readiness of this technology.

1.1 Fundamental Principle

Ultrasonic metal welding is a solid state joining process used to weld thin metal sheets, foils and wire. The principle of this welding operation follows from creation of an oscillating shear force (ultrasonic vibrations) under moderate pressure (normal force) at the interface between the mating surfaces, to separate liquids contaminants, voids, oxide layer and offer new contact at many points.

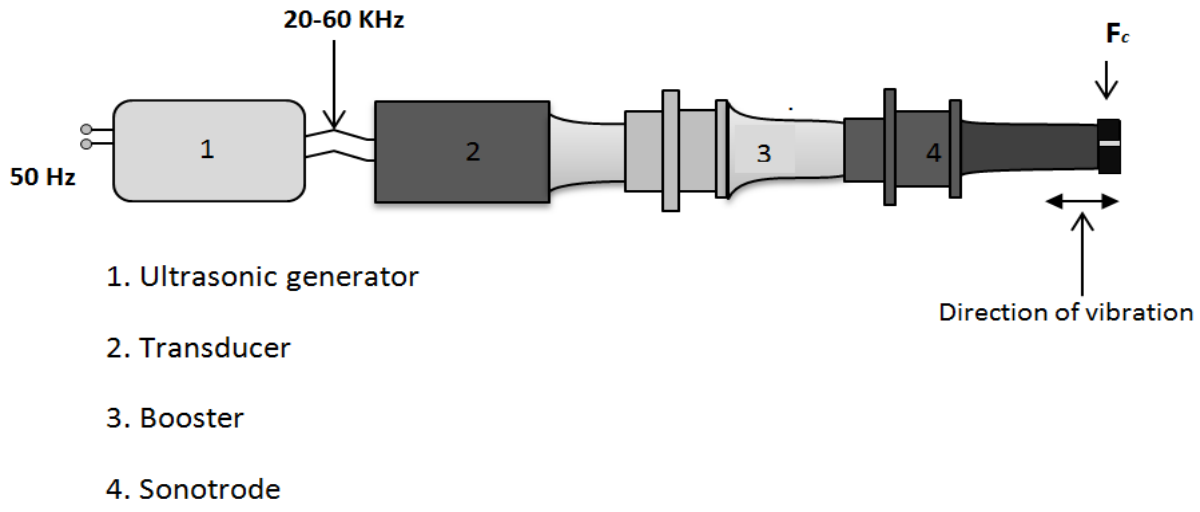

Fig. 1.1 Principle of ultrasonic welding

The vibrations are applied parallel to the weld contact area. As shown in Fig. 1 a supply of 50 Hz electrical energy is supplied to the ultrasonic generator which amplifies it up to 20 KHz – 60 KHz electrical energy and the same provided to the piezoelectric transducer which converts electrical energy into mechanical vibrations which is then enhanced by booster and transferred up to the sonotrode. When the vibrations reached to the contact area and results in oscillation causing an increase in diffusion across the weld interface and produces weld similar to that of diffusion welding. At the welding area, dynamic shear stresses are produced due to the combined effect of ultrasonic vibration and static load. The effects of interfacial slip and plastic deformation will heat the rubbing area and the temperature generated is always less than the melting point temperature of the parent material. The intense shearing and plastic deformation causes bonding of the adjacent contact surfaces. These shear forces regulate the weld quality and the power that is required to produce the joint. With the gen of the forces that act at the weld interface, it is possible to control weld strength [1].

There are mainly two types ultrasonic metal welding systems commonly used for industrial purpose. The working of the two systems was discussed in following sessions:

1.1.1 Wedge-reed system

In the wedge-reed system demonstrated in Fig. 1.2 (a), the components are the generator, transducer, and wedge and reed arrangement of segments, used to deliver the ultrasonic vibrational energy and provide it to the workpiece that are clamped between the sonotrode tip and anvil. A pneumatic, pressure driven or electrical gadget can be utilized for applying the normal force by controlling the upwards and downwards motion of the sonotrode. Typically, the amplitude which is in the range of 10 to 100 μm can be varying as per the tool design. The purpose of the wedge is to enhance the amplitude and that is transfer by the reed to the sonotrode tip. At times for the wedge-reed framework, it is desirable over plan the anvil as a vibrating part out of phase resonance, to build the movement over the workpiece [2]. Truth be told, this may expand the capacity of this kind of welding system to be utilized for high strength alloys. In this system, as the transducer is straightforwardly brazed to the reed and then specifically touches to the welds through sonotrode tip. Therefore, the transducer is equipped to drive the sonotrode and certainly does not control weld parameters.

1.1.2 Lateral Drive system

This type of ultrasonic welding system is more commonly used, as shown in Fig.1.2 (b) the system comprises of a generator, transducer, booster and sonotrode. Sometimes, the combination of sonotrode and booster which is then connected to the transducer is termed as welding stack. In a same way to the wedge-reed framework, the transducer creates a vibration of the piezoelectric plates. The booster expands the vibrational amplitude relying upon the input and serves as a mounting for the welding stack. The sonotrode can further expand the amplitude

up to the welding range. In this system, the sonotrode is attached parallel to the direction of vibration of the tool. Hence, the vibration energy is transmitted to the workpiece in a transverse way. The parts, generally sheets or foils were clamped between moving sonotrode and stationary anvil in lap configuration. The ultrasonic vibration of the sonotrode is in the parallel direction to the part surface, generating a scrubbing movement at mating surfaces. The action creates heat due to friction caused by the relative movement in the mating parts, as a result of which shear deformation occurs at the zone with subsequent weld formation.

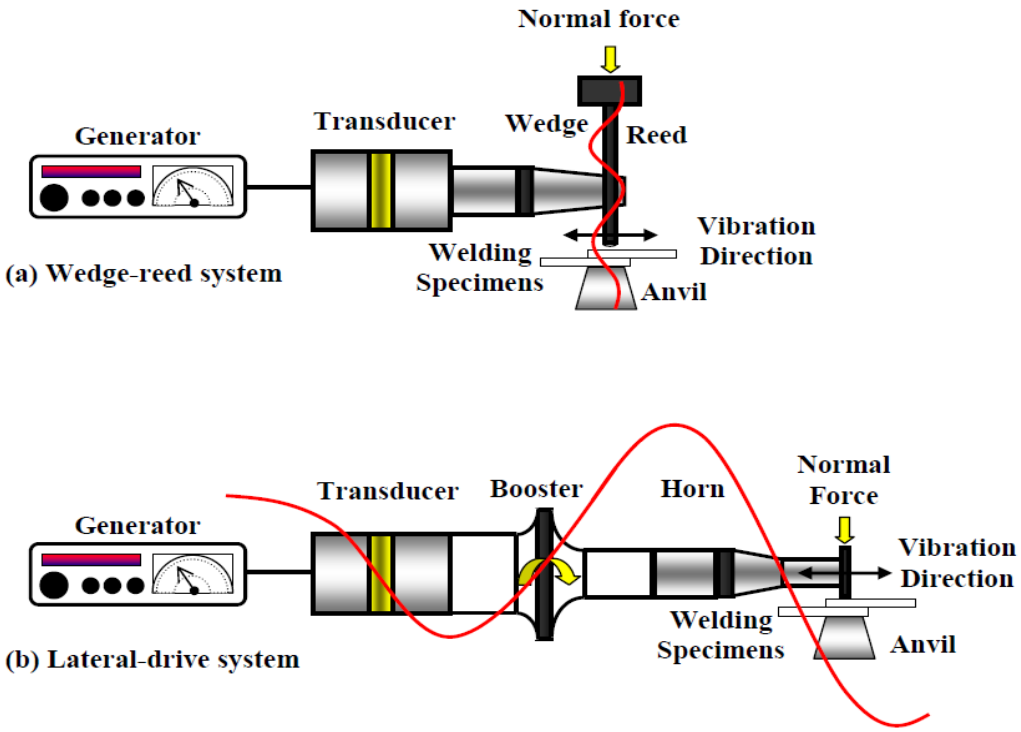

Fig. 1.2 Types of ultrasonic metal welding system, **(a)** Wedge reed system, **(b)** Lateral drive system [2].

1.3 Summary

The above chapter highlights the necessity of Ultrasonic welding in the area of manufacturing. The chapter also gives a brief idea about different types of ultrasonic welding and their uses.

CHAPTER 2

LITERATURE SURVEY

2.1 Finite element analysis

The field of ultrasonic welding is one of the deliberated topics in the manufacturing of accessories used in automotive, aerospace and electrical appliances and numerous researchers have reported their outcomes on the Finite element analysis of the mechanism, on optimization of process parameters, temperature distribution at the interface and bonding strength, etc. Some of the important observations are presented below.

Elangovan et al. [1] developed a model for the temperature distribution during welding and stress distribution in the horn and welded joints for are presented. The FE model is capable of predicting the interface temperature and stress distribution during welding and their influences in the work piece, sonotrode and anvil. It also included the effect of clamping forces, material thickness and coefficient of friction during heat generation at the weld interface. Concluded that temperature is more in the work piece than the sonotrode owing to the fact that more heat is generated in the work piece where the ultrasonic energy is focused. **Siddiq and Ghassemieh [2]** have stated that ultrasonic welding is a combination of surface friction and volume softening (plasticity). So the attempt has been made to simulate both of these effects on the metal during welding. Found that friction stresses at the weld interface decrease due to thermal and acoustic softening which is in conjunction with the experimental results and the maximum temperature reached during the ultrasonic welding is well below melting temperatures of the joining materials. **Konchakova et al. [3]** investigated for joining CFRP composites with Aluminium alloys. An FE model for damage evolution is developed for interfacial traction-separation-law based on elastoplasticity with Lemaitre-type damage. Simulations are carried out for three different interface geometries: elongated rectangle, cross rectangle and square. The study found out that damage develops slower in the specimen with square interface than in the specimen with

rectangle interface. With every load steps, the damage parameter reaches the maximum value in the specimen with the cross-rectangle interface. Comparing with experimental data shows that the damage process and the fractured zone are identical to simulated results for the specimen with the square interface. A level set based approach is taken to simulate the forming process in ultrasonic welding by **Levy et al. [4]** for thermoplastic composites. They focused their study on localized heating and flow of polymers at the weld interface which is achieved due mechanical dissipation in the energy directors at the weld interface. A simulation tool is developed using Eulerian framework which is able to handle the multi physical aspect of the process for material flow, vibration and heat transfer. The framework allows treating the large deformation of the energy director. The simulation result lets us understand the physical phenomena during welding where a fold of polymer is created that fill the gap between the two plates. **De Vries [5]** discussed the mechanics and mechanism of USMW. In this study, a mechanics based model was developed to measure and calculate the tangential forces during ultrasonic metal welding that act on the weld interface and correlate them to weld quality, the model is also capable of predicting the temperature generated during welding and the values are in good agreement with the experimental findings. It was found that interface temperature varied from 40% to 80% of the melting point depending on the value of the parameters used for welding as well as the model explains the impact of material properties and surface conditions with the process variables such as vibration normal force and amplitude on the weld behavior.

2.2 Sonotrode design for ultrasonic welding

Amin et al. [6] studied the finite-element analysis of sonotrode profile and material using CAD and suggested a new design profile with different geometry. An optimization technique has been followed to achieve maximum magnification, for greater rates of material removal and

tolerable working stresses for the sonotrode material. Concluded that the sonotrode profile conical on the upper end and cylindrical at the lower end. **Pandya et al. [7]** discussed on the design of numerous shaped acoustic sonotrodes and are used for joining of High-Density Polyethylene plastics. The theoretical dimensions were first calculated for different sonotrode shapes and compared with the dimensions found through commercial horn design software CARD. Then the response is evaluated by taking weld strength with input parameter such as pressure, Amplitude, thickness with respect to different horn profile. **Zhang et al. [8]** successfully welded two different alloys AA6111 and TiAl6V4 with high power ultrasonic spot welding and have not detected any intermetallic reaction layer which is studied with the help of an electron microscope. The parameters and their effects were studied for welding time and natural aging on peak load and fracture energy. With an increase in the weld time, peak load and fracture energy also increases and then reached a plateau. In case for lap shear strength (peak load) which performs with similar fashion for Al– Al joints and after natural aging, there is a substantial transformation occurs in the fracture mode of welds which transferred from ductile fracture to interfacial failure due to the strength regain of AA6111. **Villegas [9]** has used a flat energy director at the weld interface and relate the advantage of effect of welding process data over weld strength and taken process data such as dissipated power and displacementt of the sonotrode the whole system is applied for successfully welding of thermoplastics. The developed relationship allows the parameters to consistently result in high-strength welded joints.

2.3 Optimization of ultrasonic welding Process

Joining of Aluminium to magnesium is a big challenge because of the formation of brittle intermetallic phase but in ultrasonic welding as it operates at well below the melting point temperature, so the challenge could be solved. **Panteli et al. [10]** investigated the effect of

process parameters and energy input on joint formation between Al-6111 and Mg-AZ31 alloys. The Magnesium sheet is precoated with 50 – 100 μm thick layer of Aluminium using cold spray process. It was found out that the achieved weld strength is comparable with the Mg-Mg welding, but the joining causes an intermetallic reaction layer formation results in embrittlement at the joint with lowering the fracture energy. **Elangovan et al. [11]** conducted experiments to optimize process parameters like pressure, amplitude, and weld time and also compared the experimental value with the developed simulated results for Al and Al_2O_3. Taguchi's design of experiment methodology is implemented for the analysis. Concluded that level setting of pressure 2 bar, amplitude 45 μm and 2.5 sec weld time give the optimum weld strength of 3.30×10^6 N/m^2 after the confirmation test. The temperature at the interface is measured with the help of a K-type thermocouple and is compared with the simulated value and found to be in good agreement. **Liu and Chang [12]** have utilized Taguchi technique with L18 orthogonal array design to optimize the joint strength of ultrasonically welded thermoplastic composites. The thermoplastic materials composed of 15% to 35% glass-fiber packed nylon-6 composites. The welding is performed on a 2 kW Ultrasonic welding machine and their joint strengths of the specimen were measured by a tensile testing machine. The experimental result suggests major factors that affect the joint strength are amplitude, hold time and shape of the energy directors. Energy director with Semicircular shape found to give highest strength and also the joint strength increases with increasing the fiber content in the parts of the composites but reduces with the higher moisture of the materials. **Wijk et al. [13]** have proposed an experimental design to optimize ultrasonic welding process in series and mass production, by applying a quantitative method for evaluating product quality. As the Welding process usually have sufficient accuracy for a repeatable machine setting pertaining to weld quality. It has been shown that for the

strongest weld, the fracture due to tensile loading is not restricted to the weld interface. Alternate process parameter like time control and use of a trigger force have also been used which may give useful contribution during series and mass production by reducing the machining time. **Elangovan et al. [14]** studied the effect of process parameters and found out the optimum setting for weld strength by coupling response surface methodology (RSM) with genetic algorithm (GA) in ultrasonic metal welding. Experiments were conducted on a 2000 Watt machine as per central composite design for spot welding of 0.2 and 0.3 mm thick copper and brass materials. RSM is employed to generate an effective model to predict optimum weld strength by incorporating process parameters with levels such as pressure (at 3 bar, 3.5 bar, 4 bars), weld time (at 2.5 sec, 3.0 sec, 3.5 sec) and amplitude (28 µm, 42.5 µm, 57 µm). RSM is further attached with the GA to optimize the parameters for improved weld strength. The welding results achieved from GA were compared with experimental data and found the difference in less than 6%. **Harras et al. [15]** studied the ultrasonic welding of PEEK-carbon composites in order and determine the optimum welding conditions with parameters applied pressure and weld time. The optimum range of pressure applied at the interface was 3.8 MPa. The properties of the joint were evaluated by fracture tests with both Mode-I (opening) and Mode-II (shear). The efficient conversion of ultrasonic energy into thermal energy in the composite is very much depending upon the weld time and physical configuration of the specimen. However, the optimum joint strength to correspond to a specific value of total energy input found to be 6.8 J/mm^2. **Kim [17]** studied the process robustness of ultrasonic spot welding on thin dissimilar metal sheets. By the help of mechanical test (T-peel test) quality of the weld is evaluated and the criterion is then applied to estimate the weldability. The regression equation is

employed to find out the optimal condition. The weld quality classification and weld lobe are valuable in setting up a robust process in ultrasonic welding of thin metals.

2.2 Research Objective

From the exhaustive survey of past literatures it has been viewed that numerous works have been accounted for FE analysis of ultrasonic welding using a single sonotrode, but no one have given their concern on how the temperature and stress distribute by changing the sonotrode shape for the model. An optimization technique is also utilized to find out the optimum parameter setting and the effect of the process parameters on tensile strength of the joint. The objective of the present work is listed below:

- To develope FE model to analyze the temperature and stress distribution in ultrasonic welding.
- To study the effect of different sonotrode shape on the developed FE model.
- To find out the optimal parameter setting and effect of controllable parameters on the tensile strength of the joint by using a RSM coupled with Desirability function.
- To validate the FE model by conducting the experiments on optimal parameter setting.

CHAPTER 3

MECHANICS OF ULTRASONIC WELDING

3.1 Shear forces acting at the sonotrode tip

The chapter will be discussing the mechanics of the ultrasonic metal welding. A numerical analysis has been done for the applied loads and deformation of the workpiece, sonotrode and anvil under the same load. The figure 3.1 shows in more details about the process, where the only external force applied is the clamping force applied at the top of the sonotrode used the kept the materials in contact. As a result of the applied clamping force, the knurl pattern made on the sonotrode were inserted into the top part and helps the system to transfer vibration into the weld interface in synchronize with sonotrode. From the figure, it is shown that the not only the normal force F_N but also the net shear force F_I is also applied at weld interface as a result of the transverse vibration of the sonotrode.

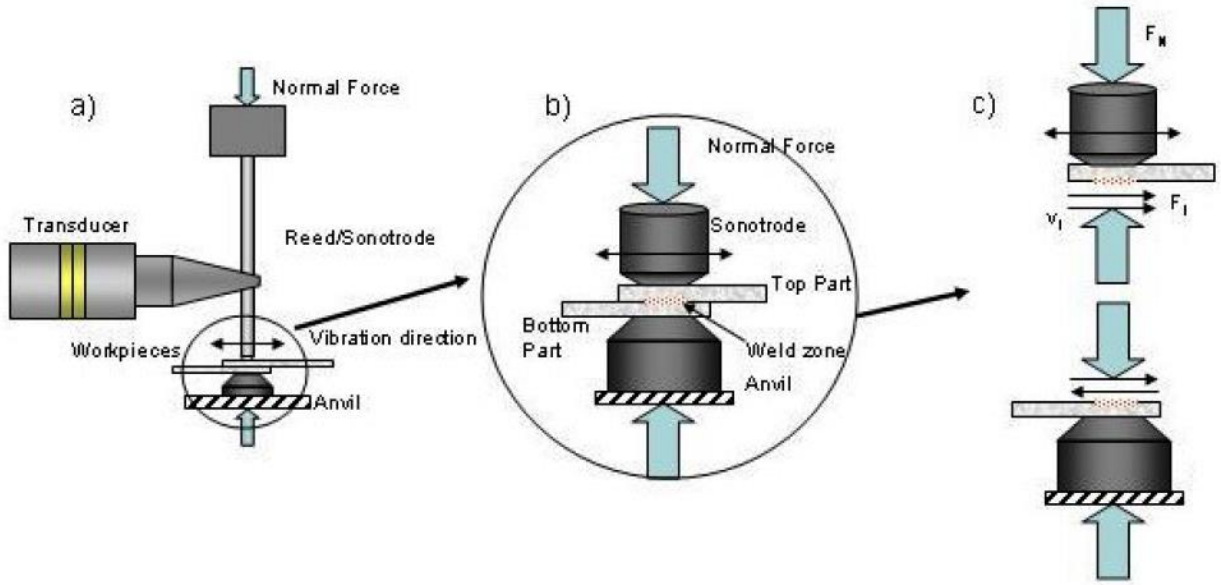

Fig. 3.1 Force morphology of the Wedge Reed System [5]

The model developed in the study is for a spherical sonotrode where the compressive stresses were not uniform and is time dependent. The study can also be applied for other shaped sonotrodes. To calculate the Shear force at weld interface we first needs to concentrate on the few factors like the component of the normal force F_N, heating of the workpiece and sonotrode

tip during welding, and the impact of the part geometry on welding. The heating caused during welding were calculated from heat flux equations at the deforming area of weld interface and the frictional area where the parts are in contact.

It has been discussed earlier that the knurl pattern made on the sonotrode tip used to prevent slipping of the part and to provide proper grip and the same combination can be seen for the bottom part and anvil. Experimentally it was found that the impact of the static force alone on the knurl pattern is negligible, it is only the tangential force during welding responsible for the above action. The indentation results in the development of complex stresses at the contact area. However, these complex stresses will be extinct within a small distance leading to a uniform stress distribution throughout the cross section but during welding the portion subject to a shear stress. Hence, a combined compressive and shearing model is assumed for the plastic deformation of the material. To analyze this combined stress Tresca's yield criteria is used as stated below:

$$Fs \leq \sqrt{\left(\left(\frac{Y(T)}{2}\right)^2 - \left(\frac{F_N}{2A_s}\right)^2\right) \times A_s} = \tau_y \times A_s \qquad (3.1)$$

Where:

F_s = Shear force at the sonotrode tip.

Y(T) = Temperature dependent yield strength

A_s = Sonotrode area in contact with the top part

F_N = Normal force on the sonotrode

τ_y = Shear yield stress

From the condition if *Fs* is less than R.H.S then top part will vibrate with the sonotrode simultaneously, but if it's equal then tip sticking will occur.

3.2 Contact stresses at interface

Contact stress is nothing but the compressive stresses generated by the sonotrode which is effectively distributed over the larger area of the top part. The magnitude of the contact stress depends upon the thickness of the top part as it spreads out with larger area. In case of a spherical sonotrode shape, the contact stress is maximum towards the center.

3.3 Shear forces at weld interface

For calculating the forces at the interface one first needs to consider the dynamics of the part geometry, as we know that at the mating part a combined shear-normal force is applied, so let us first assume both the bottom and top part are rigid and length is reduced up to the sonotrode contact area. The bottom part is fixed with the anvil while the top part moves with the sonotrode. This will allow the dynamics of the part considered single body motion, without any chances of resonance occurs for the case of the larger body. During welding, a thin area of plastic deformation is resulted with intense shearing and bonding occurs between the parts. It is considered that the top part vibrates in same amplitude with the sonotrode and same can be simply expressed as:

$$\xi(t) = \xi_0 \sin(f\,t) \tag{3.2}$$

Where:

f = frequency of vibration
ξ_0 = sonotrode amplitude

As top part oscillates with the sonotrode, so their acceleration is same and can be expressed as:

$$\frac{\partial^2 \xi}{\partial t^2} = -f^2 \xi_0 \sin(ft) \tag{3.3}$$

With the increase in deflection of the top part the sonotrode forces are also increases, hence maximum acceleration has to be considered.

$$m \times \xi_{\max} = Fs - F_I$$
$$As \times d \times \rho \times f^2 \times \xi_0 = Fs - F_I \quad (3.4)$$

Where:

ρ = density of the material

m = mass of the top part

As it said earlier that the anvil is fixed and so as the bottom part is fixed to the anvil, so anvil force F_A is equal to the interface force F_I. Now let us consider for an extended length of the part, which in a direction parallel to the vibration and the force developed is in one direction. The force for extension F_{EX} has its maximum when the deflection is maximum at the end.

$$m \times \xi_{\max} = Fs - F_I - F_{EX} \quad (3.5)$$

As top part moves with the sonotrode, so the extension of the top part is also excited by sonotrode frequency and velocity. So the force of extension as a function of part length can be expressed as follows:

$$F_{EX} = E \times A \times \frac{f}{c} \times \xi_0 \times \tan\left(\frac{f}{c} \times l\right) \quad (3.6)$$

Where:

E = young's modulus

A = area perpendicular to the vibration

c = wave velocity (longitudinal)

l = extension length

By solving the Eq 3.5 for calculating shear force Fs s compare with Eq 3.1 which says the parts has a plastic limit although it is considered to be rigid.

$$m \times \xi_{\max} + F_{EX} + F_I \leq \sqrt{\left(\left(\frac{Y(T)}{2}\right)^2 - \left(\frac{F_N}{2A_s}\right)^2\right) \times A_s} \quad (3.7)$$

Now for the interface forces

$$F_I = \sqrt{\left(\left(\frac{Y(T)}{2}\right)^2 - \left(\frac{F_N}{2A_s}\right)^2\right) \times A_s} - m \times \xi_{\max} - F_{EX} \qquad (3.8)$$

From the R.H.S of the expression which has three parts with the first part depends upon temperature and normal force, while the second is constant for a given material and geometry. Now F_{EX} will became very high for top part extension in anti-resonance case in return it will make interface force F_I very small by making the weld impossible. It is essential to have some amount of interface force for the welding to be accomplished.

3.4 Forces at weld interface

The interface forces are hugely depends upon the process of welding, so let us first discuss the welding process in brief:

Before welding the parts when comes in contact surface impurities present on surface which restricts the bonding to take place with the application of static normal force, which is not sufficient for the net plastic deformation required in zone. When the ultrasonic vibration starts the surface asperities comes in contact and undergoes a shear deformation. The process generates an adequate amount of localize heat resulting in softening of material and at the end of the total cycle the deformation spreads upto the entire area allowing metal to metal joining.

The interface area consists of three parts:

1. A_W is the weld area, where the whole plastic deformation of the material takes place and joint is formed. It can also termed as deformation zone area A_{DZ}.

2. A_{FR} is the frictional area situated adjacent to A_W, here no welding occurs but plastic deformation takes place.

3. A_{NC} non-contact area, where the surface are not in contact.

At the deformation zone area the limit for the contact stresses will be given as:

$$\frac{F_N}{A_{DZ}} \leq \frac{F_N}{A_W + A_{FR}} << \frac{F_N}{\lim \xrightarrow{A_{NC}} A_{DZ}} \tag{3.9}$$

From the Eq 3.9, $\frac{F_N}{A_{DZ}} = \sigma_s$ is the contact stress or normal stress applied at the weld zone. A differential element is assumed from the weld interface for the calculation of welding force F_W, now of critical yield shear stress can be calculated as:

$$\tau_Y(T) = \frac{dF_W}{dA} = \sqrt{\left(\frac{Y(T)}{2}\right)^2 - \left(\frac{F_N}{2A_{DZ}}\right)^2} \tag{3.10}$$

From the above Eq it has been seen that stress depends upon temperature, by integrating welding force can be calculated

$$F_W = \int_{A_W(t)} \sqrt{\left(\frac{Y(T)}{2}\right)^2 - \left(\frac{F_N}{2A_{DZ}}\right)^2}\, dA \tag{3.11}$$

With integrating time dependent weld area, as the normal stress depends upon the temperature and normal force we can calculate the welding force depending upon time, temperature and normal force:

$$F_W(T, t, F_N) = \int_{A_W(t)} \sqrt{\left(\frac{Y(T)}{2}\right)^2 - \left(\frac{F_N}{2A_{DZ}}\right)^2}\, A_W(t) \tag{3.12}$$

There are two types of frictional forces arises in the welded area and its surroundings, one is the shear force responsible for welding and other is the friction force responsible for heating the circumference but does not actively involved in joining process.

As there is also a frictional force applied at welding area along with the welding force, so the interface force will be written as $F_I = F_W + F_{FR,}$ but the frictional component of the force is

difficult to calculate as it depends upon the vibration and coefficient if friction which increases with increase in weld area. Now the frictional force can be termed as:

$$F_{FR} = \mu_s \times \sigma_N \times A_{FR} \tag{3.13}$$

where:

μ_s = coefficient f static friction.

It's very difficult calculate the Eq 3.13 as neither the exact value σ_N nor the frictional area were known. So the frictional force can also be written as:

$$F_{FR} = \mu_s \times F_N \tag{3.14}$$

When the thickness of the material increases frictional area expands along with contact stresses. As the top size reduces with both the parts considered to be rigid and surfaces in contact were undergo plastic deformation during yield conditions arrive. The expression for the compressive stress can be deliberate by the ratio of normal force to the sonotrode area/deformation zone area. The extensions of both the parts were assumed to be elastic rods. The forces acting on the surfaces are equal and opposite in direction because the bottom part along with anvil was fixed. Hence, the top part equation of motion can be written as:

$$m \times \xi_{max} = F_s - F_w - F_{FR} - F_{EX} \tag{3.15}$$

By substituting the value of Fs in Eq 3.1 and by rearranging the Eq 3.15

$$(m \times \xi_{max}) + F_w + F_{FR} + F_{EX} \leq \sqrt{\left(\left(\frac{Y(T)}{2}\right)^2 - \left(\frac{F_N}{2A_s}\right)^2\right)} \times A_s \tag{3.16}$$

It is mandatory that the L.H.S of Eq 3.16 needs to be smaller than the R.H.S; otherwise sticking of the sonotrode will takes with the top part as a result of yielding.

3.5 Heat generation during welding

A substantial amount of heat is generated in the material parts, sonotrode and anvil due to plastic deformation at weld interface during ultrasonic metal welding. This generated heat with

the change in temperature has a significant influence on material properties. The aim of this study is to generate a governing equation with the required assumption to give a good approximation for calculating the vibrational power dissipated at the weld interface.

During the initial period of welding, when the knurl pattern were engaged with top part plastic deformation also occur but very small in magnitude as compared to plastic deformation during welding so it is neglected. The heat generation is divided into two parts for the suitable evaluation of the model; one is the heat generation due to deformation of the material at the welding zone and the other is the heat generation due to friction which is confined to the surrounding of the welded zone.

3.5.1 Heat generation at the weld interface due to deformation of the material

Initially plastic deformation will start in small patches and distributed randomly across the deformation zone. Similarly the power is also distributed in evenly in patches over the entire volume of the zone. If we consider the patches are equal in size and dissipates an equal amount of power, than the total power can be calculated by integrating:

$$\frac{P_{total}}{V_{DZ}} = \frac{\int dP}{V_{DZ}} \tag{3.17}$$

For the calculation heat that is developed in deformation patches. Its needs go for a thin layer of shear elements at the plastic deformation zone. The shear element which is elastic in property with the work done on strained volume is given by product of shear angle and shear stress. This can assumed to be highest stress for the case of perfectly plastic material with no work hardening. Hence, the work done on the deformed volume can be written as:

$$\frac{dW}{dV} = \tau_y \times \gamma \tag{3.18}$$

where:

γ = angle of deformation

The work done on the deformation volume is for a particular period of time is equal to the change in angle during the same amount of time, which can be explained by the ratio of top part deflection to the thickness of the deformed layer.

$$\frac{\Delta dW}{\Delta t} \times \frac{1}{dV} = \tau_y \times \frac{\Delta \xi}{\Delta t \times dy} \tag{3.19}$$

As we know that the rate of change of work done is the power, similarly the rate of change of amplitude is the average acoustic speed for amplitude of ξ_0 and frequency of f_w id given by:

$$\begin{aligned} &\frac{\Delta W}{\Delta t} = P \\ &\frac{\Delta \xi}{\Delta t} = v_{avg} = \frac{1}{T}\int_0^T \left| f \times \xi_0 \cos(ft) \right| = 4 \times \xi_0 \times f_w \end{aligned} \tag{3.20}$$

Where:

f = frequency Vibration

T = time period of vibration

By substituting the Eq 3.20 in Eq 3.19 and solving, we can get the expression for power dissipated:

$$\frac{dP}{dV} = \tau_y \times \frac{v_{avg}}{dy} \tag{3.21}$$

As the deformed element thickness is constant, so the differential volume dV can be substituted by dA × dy with multiplying both side by dy one can get:

$$\frac{dP}{dA} = \tau_y \times v_{avg}$$

or $$dP = \tau_y \times v_{avg} \times dA \tag{3.22}$$

Now, by substituting the value of average differential power from Eq 3.22 in Eq 3.17:

$$\frac{P_{total}}{dA} = \frac{\int dA \times \tau_y \times v_{avg}}{V_{DZ}} \tag{3.23}$$

Similarly for the Eq 3.10 the integration would be applied for weld area A_w with respect time and by replacing V_{DZ} by $A_{DZ} \times dy$ and multiplying both side by dy:

$$\frac{P_{total}}{A_{DZ}} = \frac{\tau_y \times A_w(t) \times v_{avg}}{A_{DZ}} = \frac{F_w(t) \times v_{avg}}{A_{DZ}} \tag{3.24}$$

Now the expression 3.24 gives the amount of vibrational power which generated due to plastic deformation in the welding zone area. As we know that the heat flux is the power dissipated over unit area, so the Eq 3.24 can be rewritten by putting the value of weld force from Eq 3.12 and also the average speed from Eq 3.20, the expression for the heat flux in the deformation zone area can be written as:

$$Q_w = \frac{\sqrt{\left(\frac{Y(T)}{2}\right)^2 - \left(\frac{F_N}{2A_{DZ}}\right)^2}\, A_W(t)}{A_{DZ}} \times 4 \times \xi_0(t) \times f_w \tag{3.25}$$

From the expression, the time dependence of the amplitude is only for the initial period of the weld cycle, during this period the amplitude of the sonotrode is not equal to amplitude at the weld interface.

3.5.2 Heat generation in the weld interface due to friction

Heat generation in the surrounding of the welded zone can be calculated by the ratio of power dissipated per unit frictional area. The power dissipated can simply expressed by the product of average speed to the friction force:

$$\frac{P_{FR}}{A_{FR}} = F_{FR} \times v_{avg} \tag{3.26}$$

Now, substituting the value average speed from Eq 3.20 and the value of friction force form Eq 3.14, one can get the expression for the heat flux due to friction as:

$$Q_{FR} = \frac{\mu_s \times F_N \times 4 \times \xi_0(t) \times f_w}{A_{FR}} \tag{3.27}$$

The heat flux due to friction is needs to be applied outside the weld area at the friction area, which is assumed to be twice the radius of weld area. The average interface speed is also changes by the shear deformation which is used in both the heat flux equations; the average speed needs to be considered as constant for most part of the weld cycle.

3.6 Summary

The material properties chosen were temperature dependent, which means at elevated temperature the material property will be also changed. The forces applied on the sonotrode and welded parts were estimated with a good approximation.

The heat flux equations were generated by keeping in mind for all computation aspects and not being limited to an approximate solution. As a result of the one can numerically estimate the temperatures that will be generated at the weld interface and the sonotrode.

CHAPTER 4

FINITE ELEMENT MODELLING:

ULTRASONIC WELDING

Finite element modeling (FEM) is a numerical method to find out the approximate solutions of the given problem. It divides the complex problems into simpler parts called finite elements. It helps in getting to obtain the appropriate solution for the define problem. There were various FEM based software in the present scenario such as ANSYS, SYSWELD, ABACUS, PROE, DEFORM, etc.

In this chapter, ANSYS software has been implemented for the FE analysis of the developed numerical model. The analysis is carried out in two parts, first for the temperature distribution due to heat generation during welding and the second for the stress distribution due to applied clamping force.

4.1 Assumptions for the FE model

The following assumptions are made during analysis and the standard weld coupon used in this study is as per the resistance spot welding.

i. The sonotrode used in this analysis had a uniform circular cross-section at the tip.

ii. The workpiece are in perfect contact (no air gap).

iii. At the end of the weld, the area of the sonotrode A_S will be equal to the area of the deformation zone A_{DZ} and will be equal to the area of the weld A_W ($A_S = A_{DZ} = A_W$).

iv. The ambient temperature is assumed to be uniform and it is taken as 30 ◦C.

4.2 Modeling the temperature distribution

The temperature distribution modeling in weld interface, sonotrode, anvil is attempted in this study. A Two-dimensional rectangular Co-ordinate system was chosen due to complexity of the model. The different material properties (ASM Handbook volumes 1 and 2, 1998) considered in the present study for work piece, sonotrode, and anvil are presented in Table.1.

Table 4.1 Thermal and Physical properties for workpiece, sonotrode, and anvil

Material	*Thermal conductivity (k) in W/m^{0}c*	*Specific heat (C) in J/kg^{0}c*	*Density (ρ) in kg/m^3*	*Young's modulus (E) in GPa*	*Poisson's ratio*	*Co-eff. Of thermal expansion in $^0C^{-1}$*
Steel(sonotrode, anvil)	24.3	460	7800	210	0.3	1.51×10^{-5}
Al(workpiece)	183	896	2700	70	0.35	2.43×10^{-5}

4.2.1 Heat flux due to deformation

The expression which has already been derived in Eq 3.25 is used for the calculation of heat flux in the deformation zone.

$$Q_w = \frac{\sqrt{\left(\frac{Y(T)}{2}\right)^2 - \left(\frac{F_N}{2A_{DZ}}\right)^2}\, A_W(t)}{A_{DZ}} \times 4 \times \xi_0(t) \times f_w$$

As shown in Fig. 3.2, the variation of yield strength is experimentally found out by De Varies [5]. So the average temperature dependent yield strength for a temperature limit of 0 to 600 is given as follow:

$$Y_T = \frac{\left[\int_0^{600} (-0.649T + 326.5)\times 10^6\, dT\right]}{\Delta T} \tag{4.2}$$

$$= \frac{\left[\left((-0.649T^2/2) + 326.5T\right)\times 10^6\right]_0^{600}}{\Delta T}$$

$$= 83.126\times 10^6\ N/m^2$$

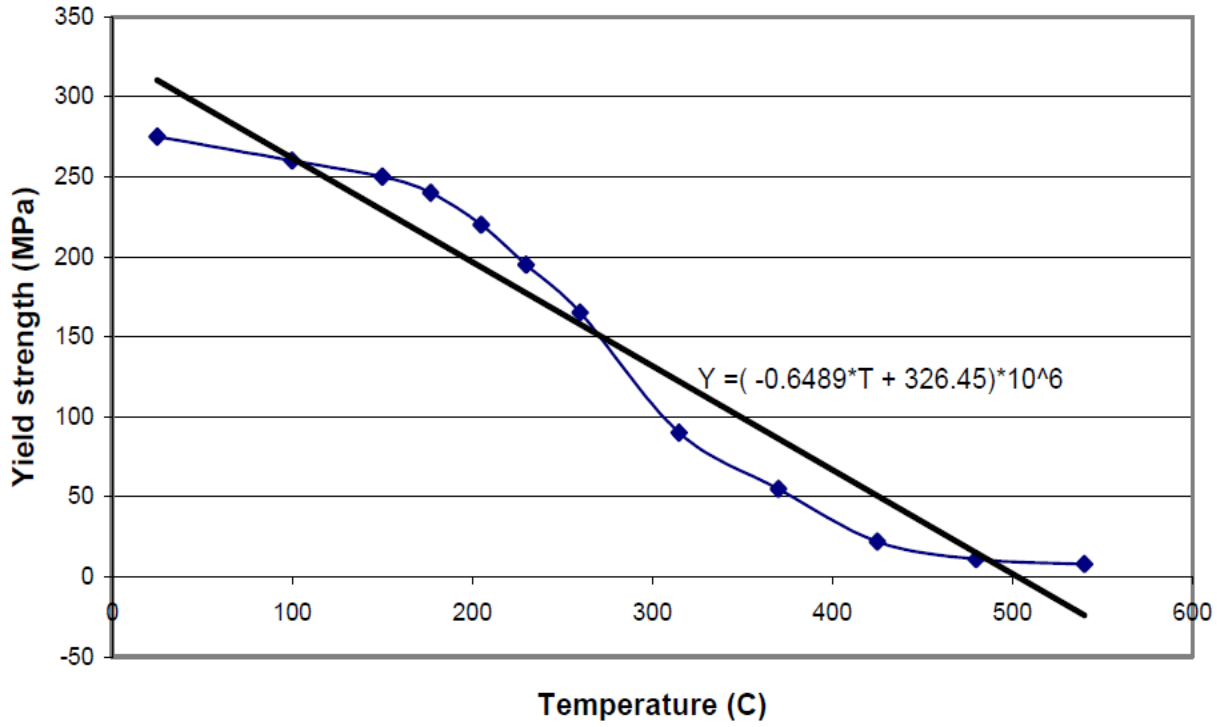

Fig. 4.1 Yield strength variation with respect to temperature [5]

So the heat flux due to deformation for a clamping pressure of 1.8 bar is given by

$$Q_w = \sqrt{\left(\left(\frac{83.125\times10^6}{2}\right)^2 - \left(\frac{1.8\times10^5}{2}\right)^2\right)} \times 4\times37\times10^{-6}\times20000$$
$$= 12.30\times10^6\, W/m^2$$

4.2.2 Heat flux due to friction

The expression for heat flux due to friction is derived in Eq 3.27, for a clamping force of 17.82 N, coefficient of friction of 0.3 amplitude of 37 µm corresponding to 80% dB, by putting all these values:

$$Q_{FR} = \frac{\mu\times F_N\times4\times\xi_0\times f_w}{A_{FR}}$$
$$= \frac{0.3\times17.82\times4\times37\times10^{-6}\times20000}{99\times10^{-6}} = 2.82\times10^6\, W/m^2$$

The above calculate value of heat flux due friction is applied to the friction area which is two time the deformation zone area.

4.3 Simulation of FE model

Fig. 4.2 shows the dimension and boundary conditions for the for the developed axisymmetry model used for the analysis in ANSYS® APDL. It is shown in the figure that deformation area from origin upto 2.5 mm where the heat flux due to deformation is applied and from 2.5 mm to 5 mm heat flux due to friction is applied. The thickness of the sheet is chosen as 0.5 mm of commercial available Aluminum sheet, while sonotrode and anvil material is chosen as mild steel. The material properties for the required thermal analysis and structural analysis are listed in Table 4.1.

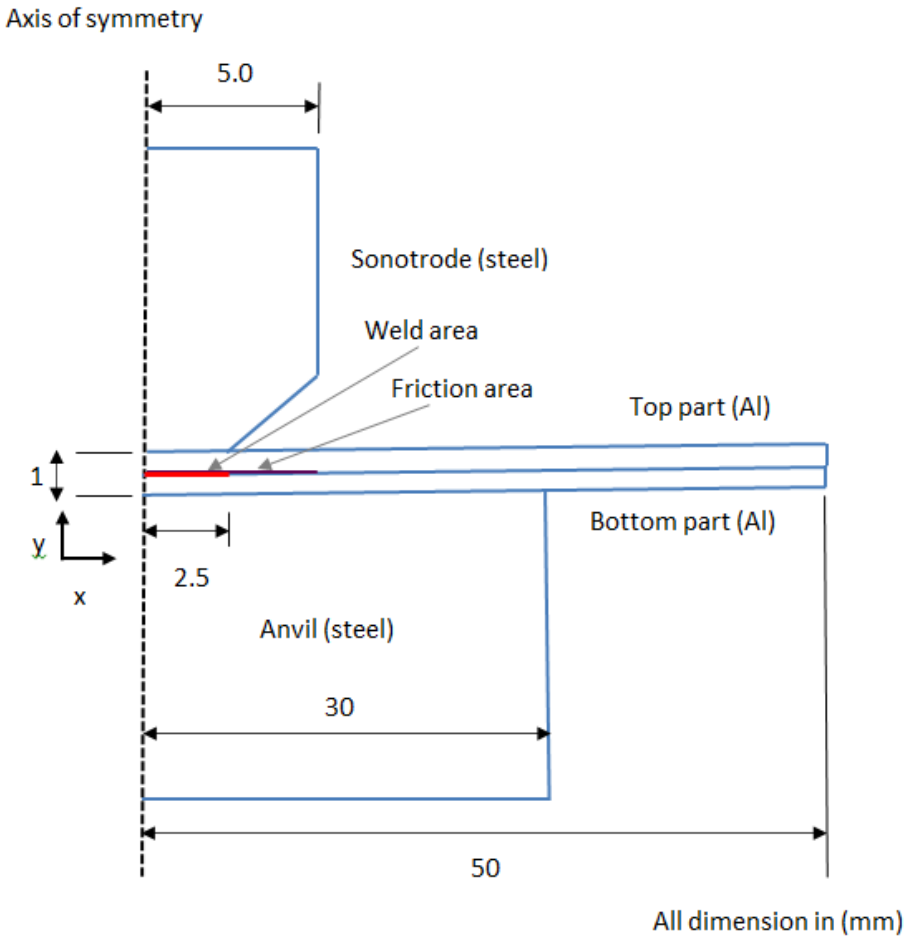

Fig. 4.2 Axisymmetry model with boundary conditions.

4.3.1 Boundary conditions

- The initial condition for temperature T_0 is assuming room temperature as 30^0.
- The heat loss due to convection to the surrounding is applied at the surface areas of the material parts which have not in contact with either sonotrode or anvil are listed below, as shown in Fig. 4.3. The convection heat coefficient is assumed as 5 J/m^{0}C.
- Q(conv.) = Q(50, Y), $0 \le y \le 0.5$
- Q(conv.) = Q(50, Y), $0 \le y \le -0.5$
- Q(conv.) = Q(x, 1), $2.5 \le x \le 50$
- Q(conv.) = Q(x, -1), $30 \le x \le 50$

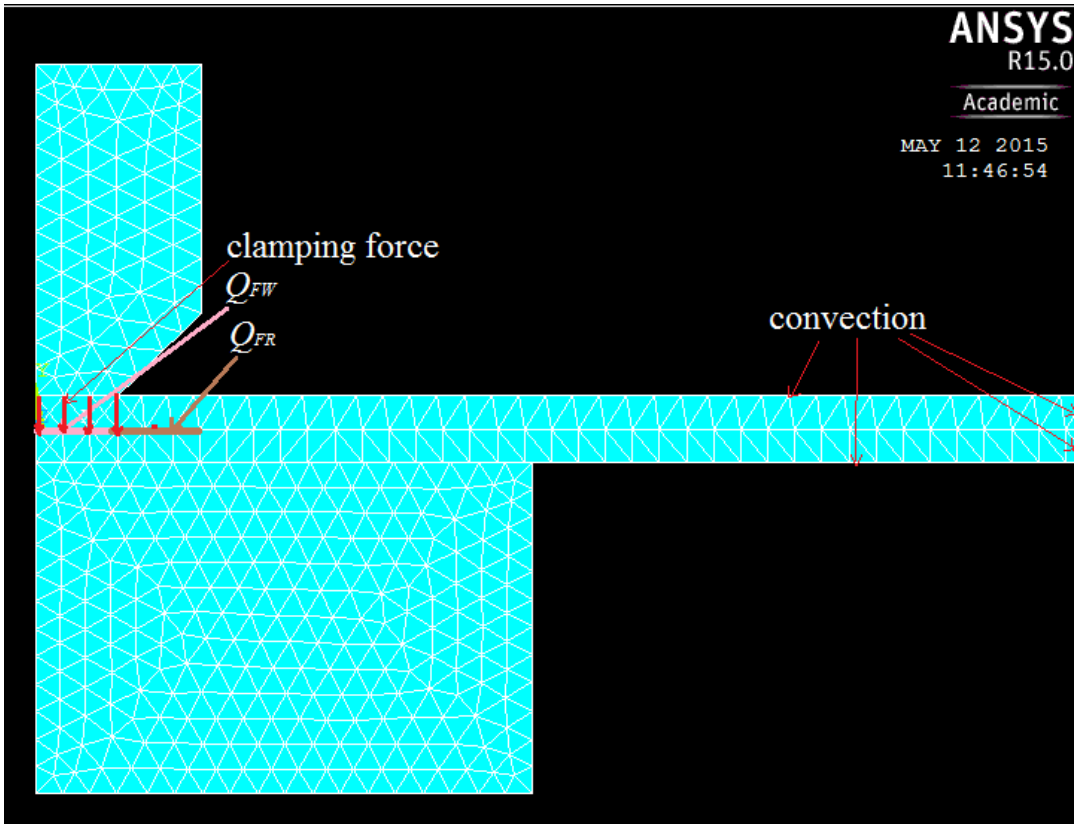

Fig. 4.3 Elementary view of the FE model with applied loads.

4.3.2 Transient thermal analysis

The contact resistance of the faying surface is a component of burden, temperature and normal yield quality in contact materials. A triangular six-noded 2D structural solid element

(plane 35) is chosen performing thermal analysis. The triangular shape makes it appropriate to model unpredictable mesh. Fig. 4.4 shows the shape, node position, and the coordinate system of the element. It has one degree of freedom, temperature change at every node. The 6-noded thermal element is pertinent to a 2-D transient or steady state thermal investigation. The mesh size picked was fine and contact is created between sonotrode with the top surface of workpiece, top workpiece with bottom workpiece, and bottom surface of workpiece with anvil.

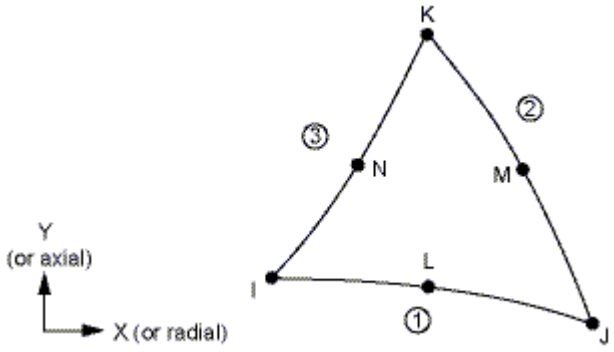

Fig. 4.4 Shape and position of nodes for Plane 35 element

A surface to surface contact is established with the help of a 2-D three noded contact element (CONTA172) and 2-D target segment (TARGE169) was utilized to denote the respective contact surfaces. The simulation is first carried out for conical shape sonotrode and then extended to exponential shape and stepped shape.

As shown in Fig. 4.3, the thermal loads like heat flux due to deformation were applied in weld area of 20 mm^2 while the heat flux due to friction was applied in frictional area 60mm^2. The loss of heat due to convection was applied on the borders of the parts, which are not in contact with either sonotrode or anvil. For 2-D geometry, the areas are assumed to be lines. A full transient analysis was carried out for a time period of 0.5 sec with time steps of 0.1 sec.

4.3.3 Transient stress analysis

The clamping force is applied on the nodes of the sonotrode as shown in Fig. 4.3, which are in contact with the top surface of the workpiece. The displacementt of the anvil is set as zero in

all degrees of freedom. The element type is switched from thermal to structural for the Plane 35 element, and that is converted to a six-noded 2-D triangular structural solid (plane 2). The node location, shape and geometry of the plane are similar to the Fig. 4.4. Full transient analysis was chosen with time step size of 0.001 for a time period of 0.5 sec.

The simulation was repeated for three different shape of the sonotrode with constant material properties and dimension of the work piece and anvil. The results gathered from the structural and thermal analysis were presented in the subsequent section.

4.4 Result and discussion

4.4.1 Temperature distribution in the model

As discusseda earlier, the simulation was carried out for three different models having different shape of the sonotrode and the resultsware presented in this ssection. The maximum temperature reached for the conical shape is 169.238 ^{0}C at the end of weld time for a pressure of 1.8 bars. Fig. 4.5 shows the distribution of temperature for a conical shape sonotrode. It shows that the temperature reaches its maximum at the deformation zone and spreads more in the workpiece as compared to the sonotrode and anvil; this is because of the fact that the thermal conductivity of Aluminum is more as compared to mild Steel. The sonotrode and anvil experience a maximum temperature of 152.656 ^{0}C.

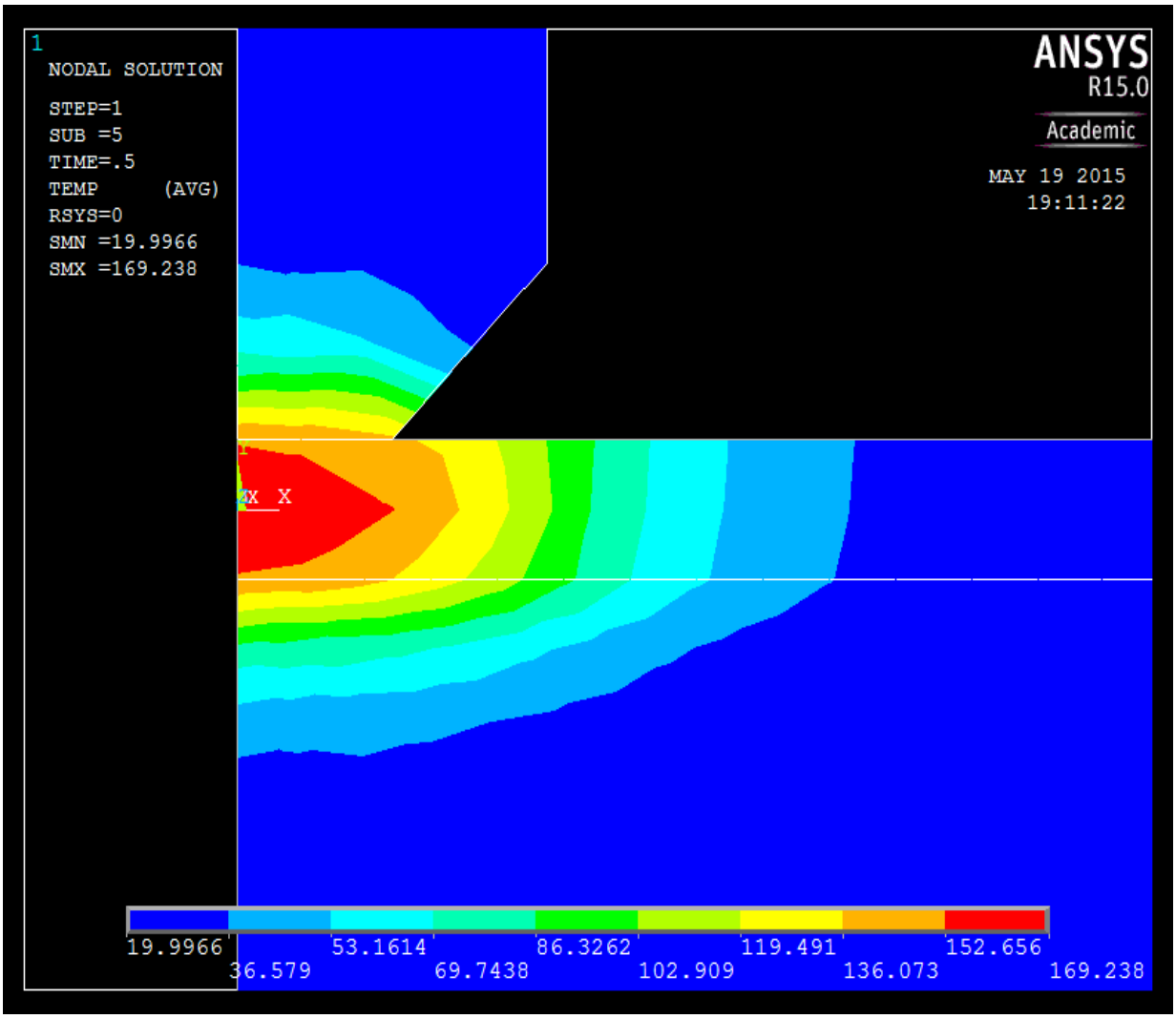

Fig. 4.5 Temperature distribution in the model with conical shaped sonotrode

Fig. 4.6 shows the distribution of temperature in an exponential shaped sonotrode with a maximum temperature of 171.439 ^{0}C at the end of the weld time. The maximum temperature in the sonotrode and anvil have reached upto 154.612 ^{0}C.

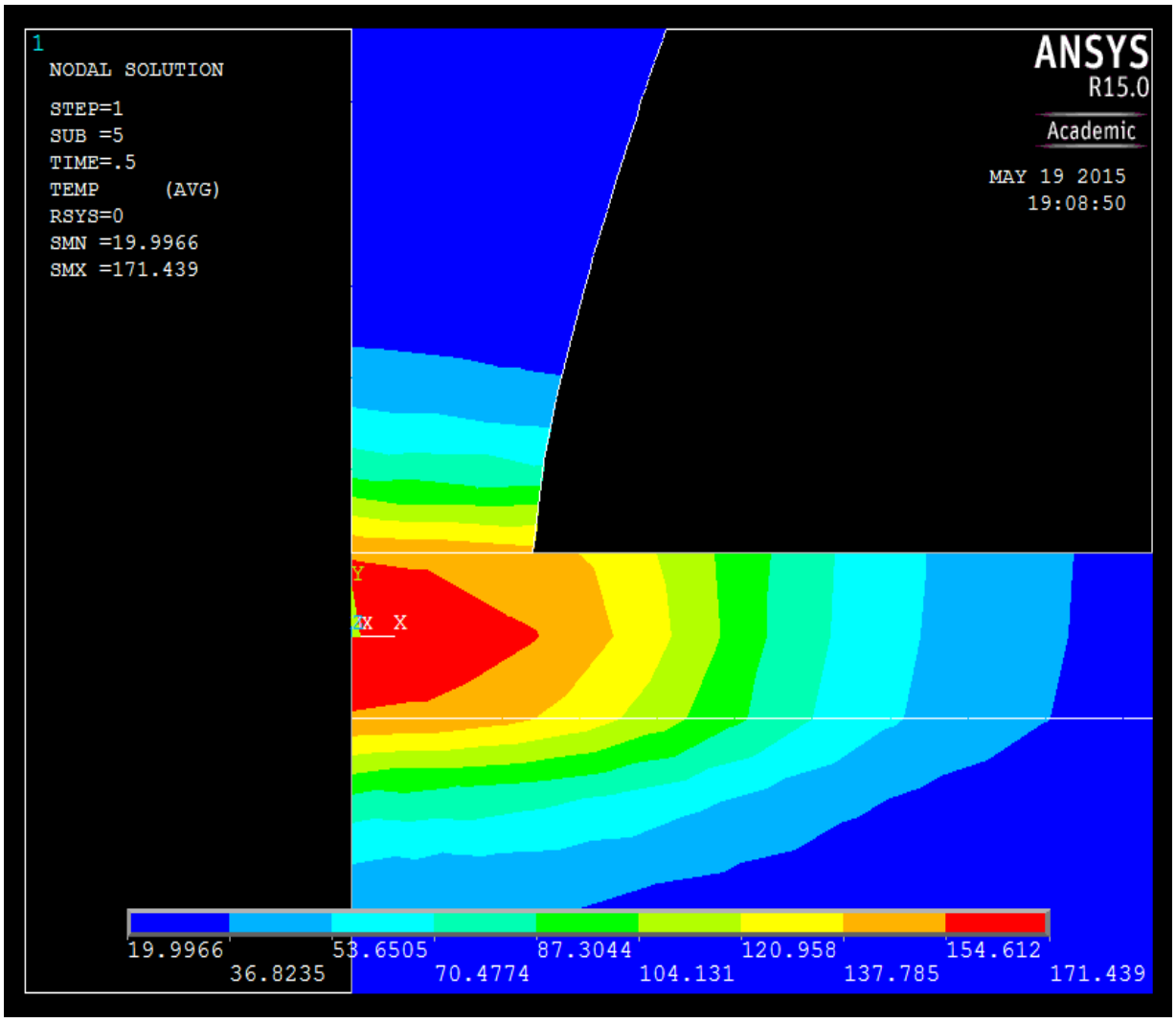

Fig. 4.6 Temperature distribution in the model with exponential shaped sonotrode

Fig. 4.7 shows the distribution of temperature in a stepped shaped sonotrode with a maximum temperature of 182.069 ^{0}C at the end of the weld time. The maximum temperature in the sonotrode and anvil have reached upto 165.171 ^{0}C.

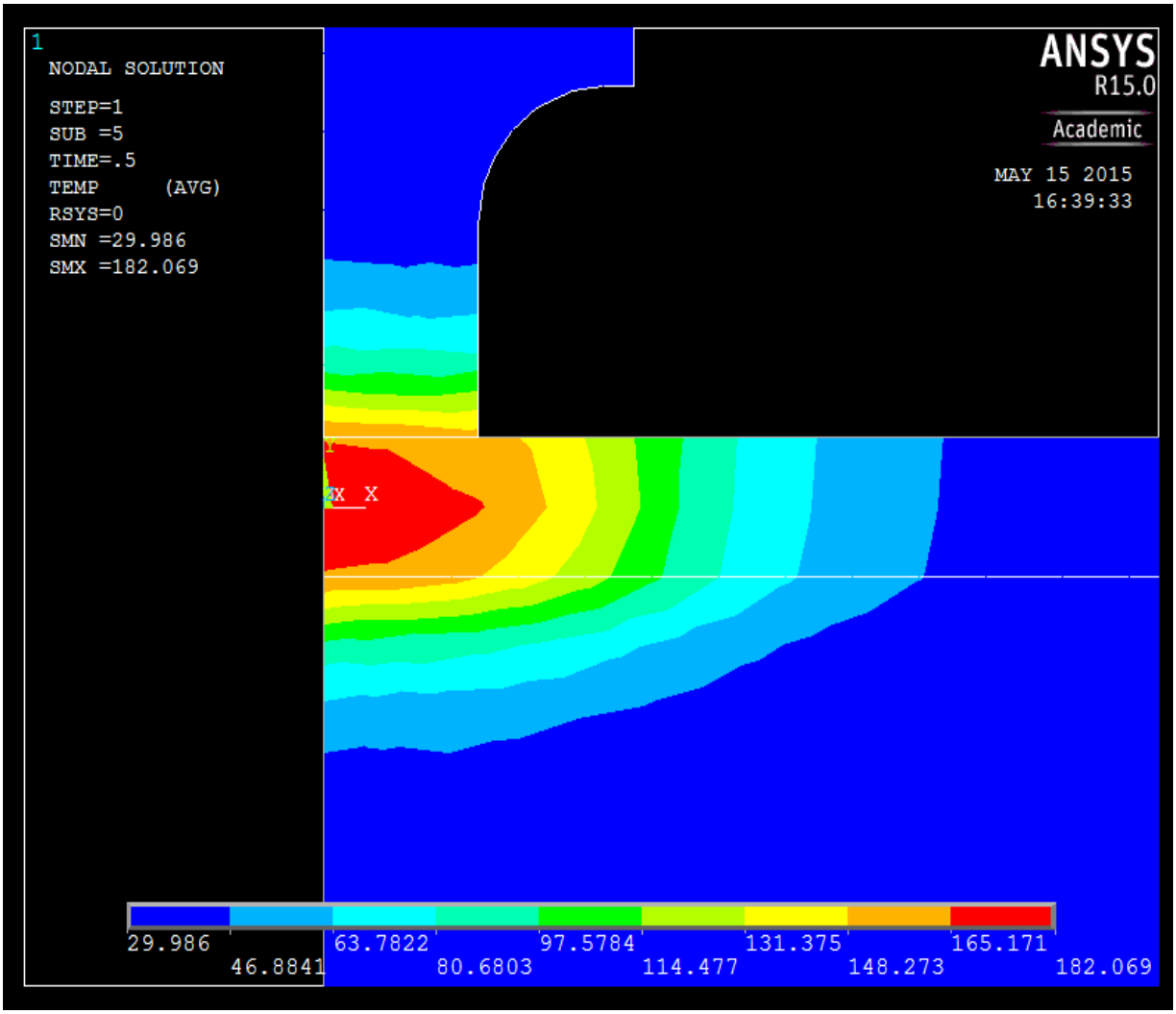

Fig. 4.7 Temperature distribution in the model with stepped shaped sonotrode

Fig. 4.8 shows the temperature variation with workpiece thickness. The variation ofttemperature from the center of the weld to the top or bottom surface of the workpiece is around 18.019 ^{0}C along the vertical direction. This observation can be used to forecast the area of heat affected zone in Y direction.

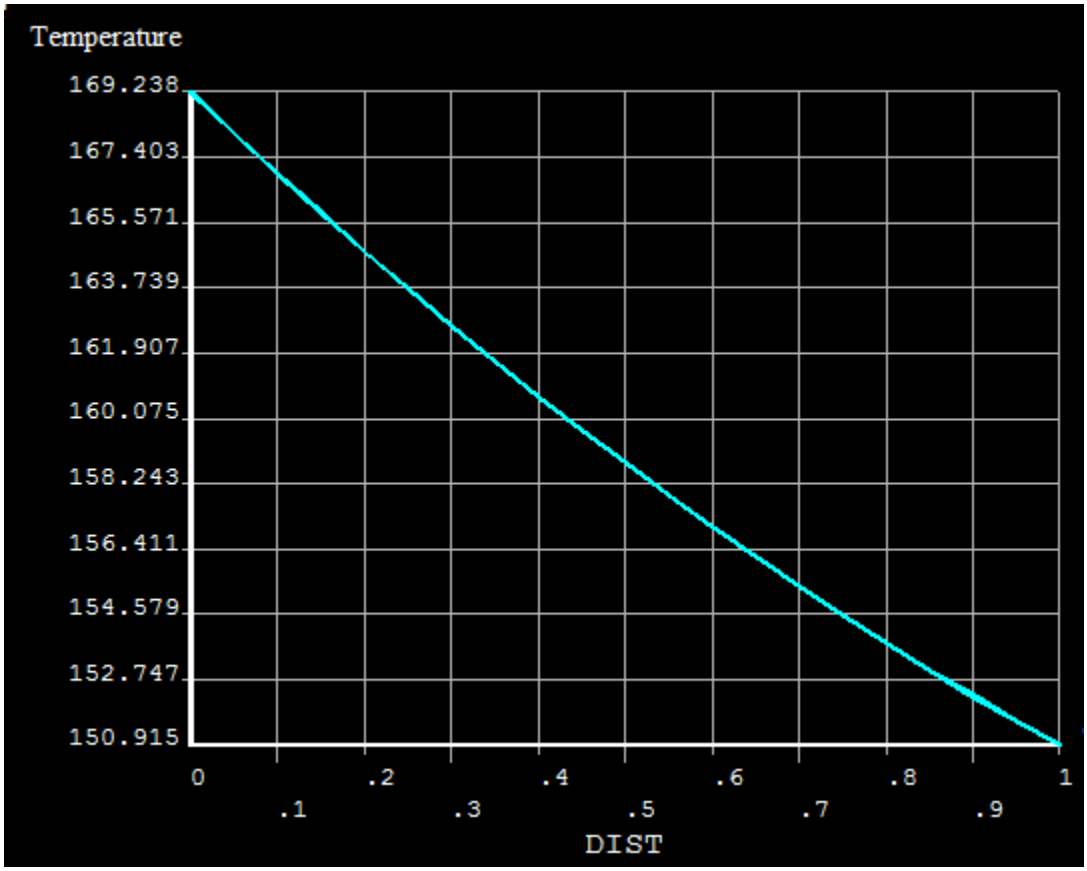

Fig. 4.8 Temperature variation in the workpiece thickness

Fig. 4.9 shows the change of temperature from origin to distance of 30 mm along X-direction. It can be seen that magnitude of temperature rapidly rises from a distance of 10 mm to the origin. The temperature in the figure is exactly from the weld interface. Fig. 4.10 shows the rise in temperature with each time step during welding in the weld interface. From the figure it can be summarized that the rise in temperature is directly proportional to the welddtime during welding.

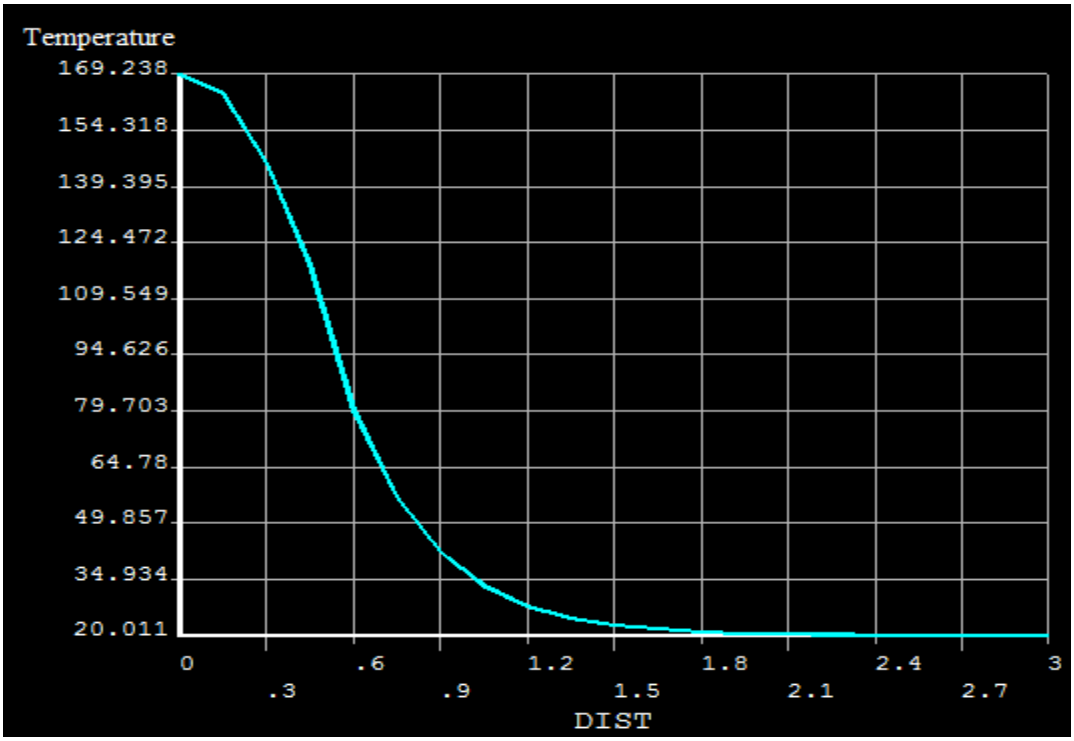

Fig. 4.9 Temperature variation in weld interface along X-direction

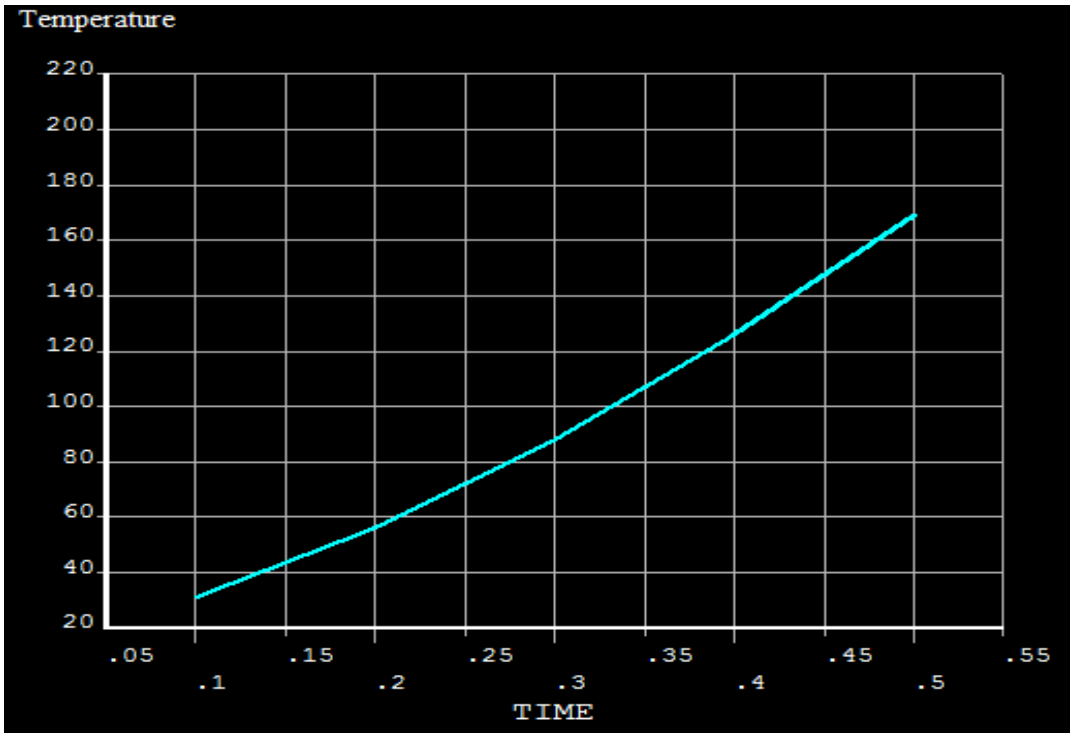

Fig. 4.10 Temperature variation in the weld interface with each time step

4.4.2 Stress distribution in the model

Similar to the thermal analysis, the simulation was carried out for three different shape of the sonotrode and the resultsware presented in this ssection. The maximum Von Mises stress reached for the conical shape is $5.31\times10^{6}\, N/m^{2}$ at the end of weld time. Fig. 4.11 shows distribution of stress for a conical shape sonotrode. It shows that the stress is maximum at the point of action of the clamping force, where the sonotrode meets with the top surface of the work piece and also in the bottom part where it touches the top surface of the anvil.

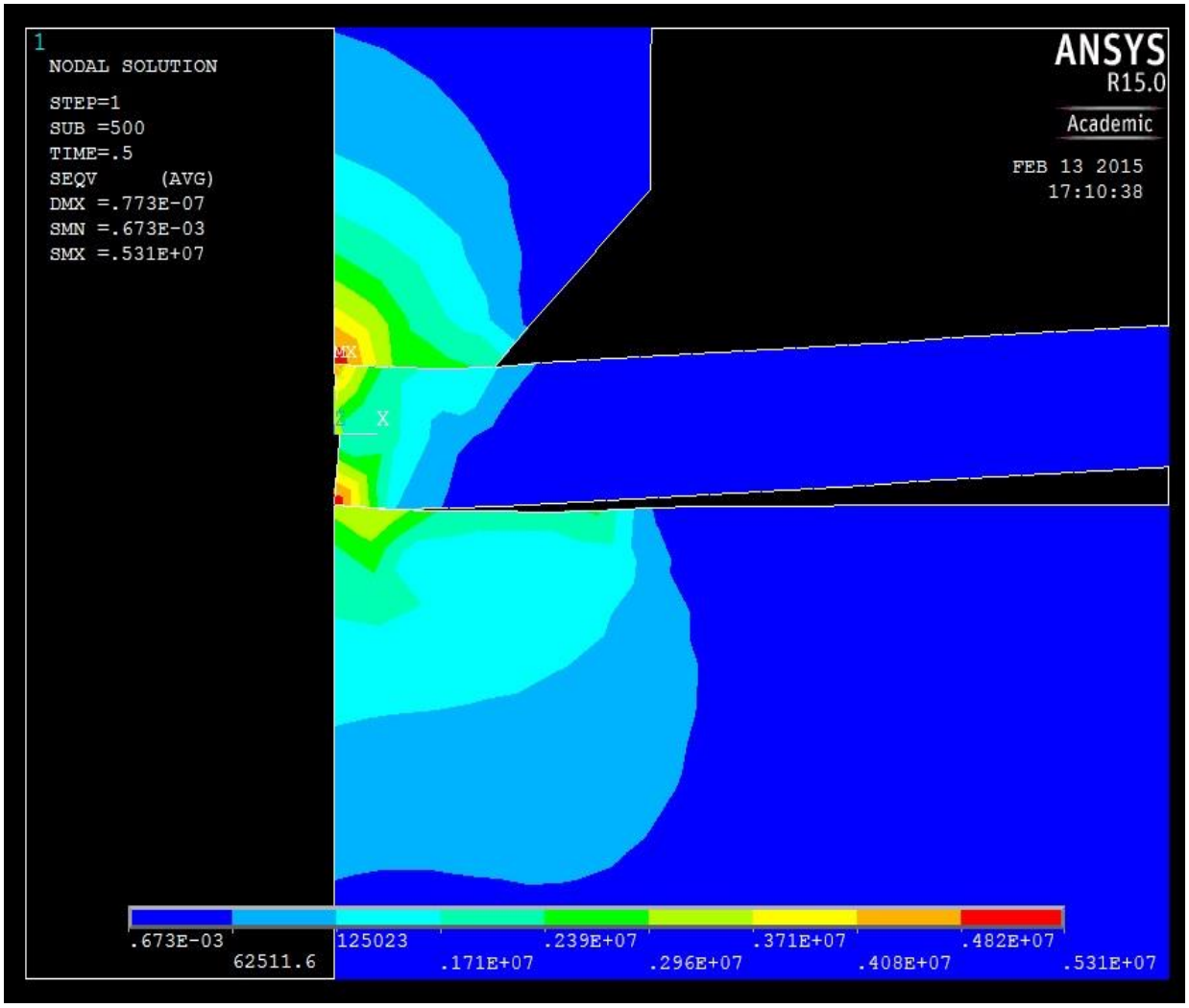

Fig. 4.11 Stress distribution in model with conical shaped sonotrode

It can be seen, with the application of force the bottom work piece moves away from the anvil during welding. This could be because of improper clamping method adapted during welding. So a proper fixture needs to be design to hold the parts during welding. Fig. 4.12 shows the distribution of Von Mises stress in an exponential shaped sonotrode with a maximum of $5.82 \times 10^6 \, N/m^2$ at the end of the weld time.

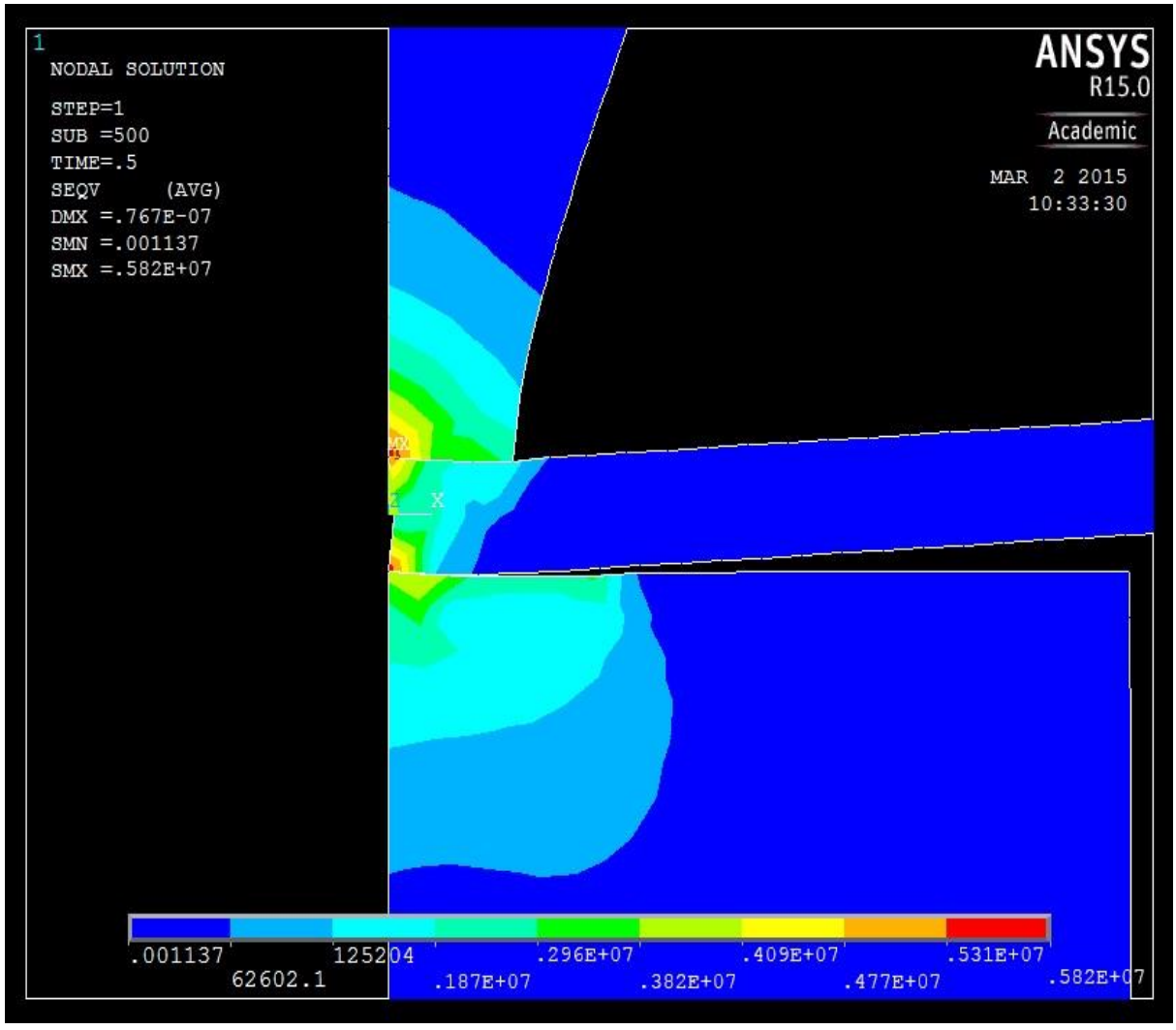

Fig. 4.12 Stress distribution in model with exponential shaped sonotrode

Fig. 4.13 shows the distribution of Von Mises stress in an exponential shaped sonotrode with a maximum of $6.27\times10^{6}\ N/m^{2}$ at the end of the weld time. It can be seen from the figure that the Von Mises stress is more intense at the sonotrode because of the complexity of the model.

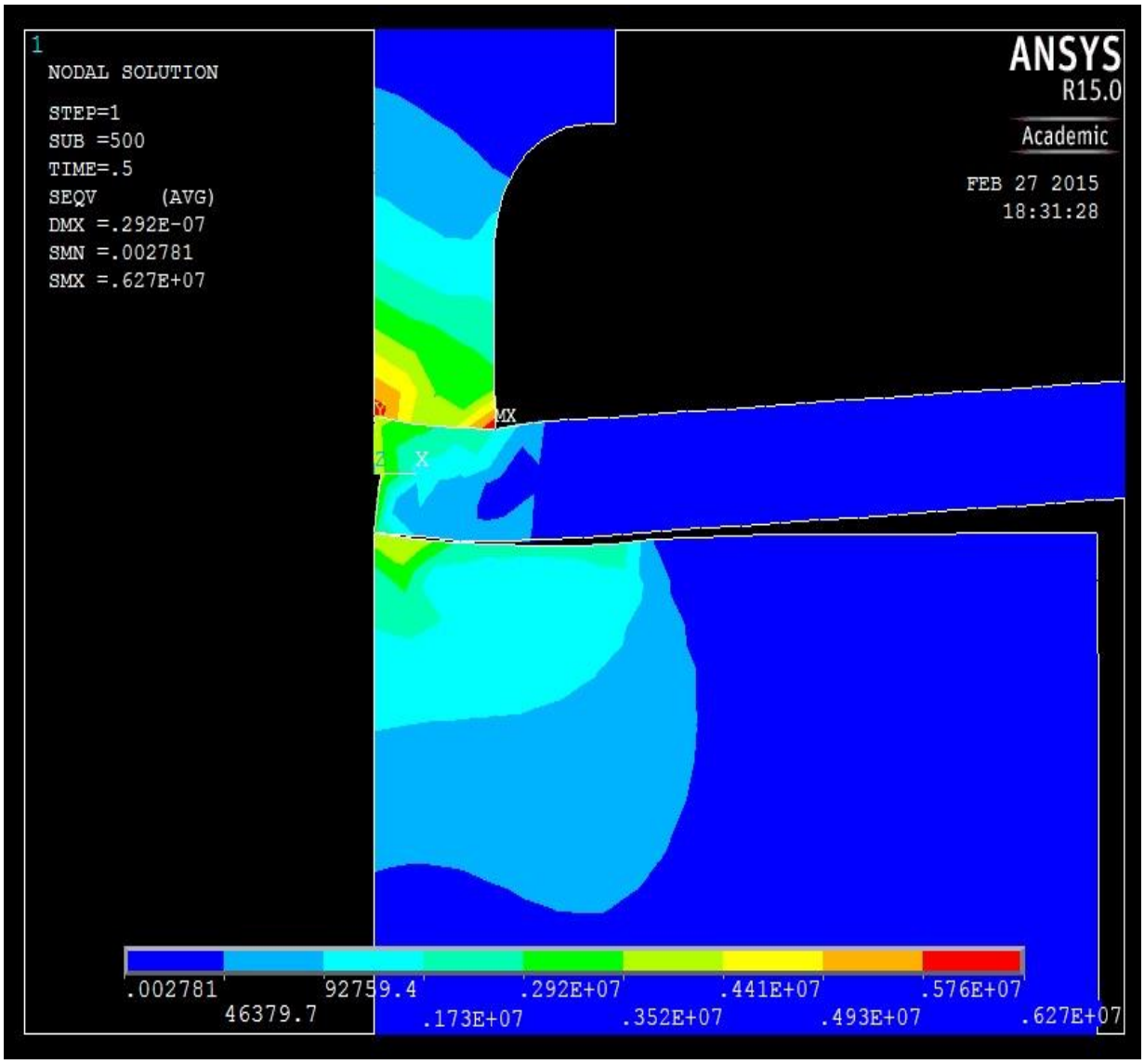

Fig. 4.13 Stress distribution in model with exponential shaped sonotrode

4.5 Summary

In this chapter, FE based numerical analysis has been performed for ultrasonic welding process using ANSYS. The value of temperature generated during simulation is compare to experimental value and it was found that the mean relative error of less than 3.4%, which shows the adequacy of the numerical model. The amount of temperature and stress generated during welding is tabulated in Table 4.3.

Table 4.3 Temperature and stress distribution from the numerical model

Sonotrode Shape	**Temperature in ^{0}C**	**Von Mises Stress in N/m^2**
Conical Shape	169.238	5.31×10^6
Exponential Shape	171.439	5.82×10^6
Stepped Shape	182.069	6.27×10^6

CHAPTER 5

EXPERIMENTATION AND OPTIMIZATION TECHNIQUE

5.1 Response Surface Methodology

It is a statistical tool used to establish a relationship between several controllable variables with one or more responses. The method was introduced by G.E.P. Box and K.B. Wilson. A series of experimental run are performed within the selected range to identify the best set of parameters which gives the optimum result for response variables. It assumes a second-degree polynomial consists of factors with coefficients for analysis. If the response variable linearly depends upon the factors, then it can be articulated by a first order polynomial but if there is any curvature in response surface then a second order model should be followed. A second order polynomial with Z as response variable is expressed by:

$$Z = \pm a_0 \pm a_1 x \pm a_2 y \pm a_3 x^2 \pm a_4 y^2 \pm a_5 xy \pm e \tag{5.1}$$

where:

Z = response variable

x, y = controllable factors

e = experimental error

a_0, a_1, a_2 … = coefficients

In this work, from the vast literature survey three controllable factors such as pressure, amplitude, welding time at three levels were selected for conducting the experiment. A Box Behnken Design (BBD) is considered which gives a total of 17 experimental runs with 5 center points. Tensile strength of the welded joint is chosen as the response. The Factors and their levels are listed in Table 5.1.

Table 5.1 Factors with levels

Factor	Unit	Levels		
		-1	0	+1
Pressure	Bar	1.4	1.6	1.8
Amplitude	%	21	24	27
Weld time	Sec	0.4	0.45	0.5

5.1.1 Experimental Procedure

The experiments were performed on 3000 W, 20 KHz ultrasonic welding machine on a 0.5 mm thickness Aluminum sheet, the experimental setup is shown in Fig. 4.11. The pressure required for the welding is received from a compressor, where the maximum limit is set up to 18 bar prior to the welding. The holding time for the experiment is set as 0.3 sec. On the contact surface of the anvil and sonotrode knurl pattern were made to prevent sliding of the workpiece during welding. Fig. 5.1 shows, specimens prepared for welding as per ASTM standards (D1002-01) [17]. Prior to the welding, the specimens were thoroughly cleaned with acetone to remove the surface impurities which can affect the joint strength. For each factorial combination, two trails of welded specimens were generated and the average of both the trials were also calculated and tabulated in Table 5.2. Fig. 5.2 shows the ultrasonically welded specimens of 0.5 mm Aluminium sheet.

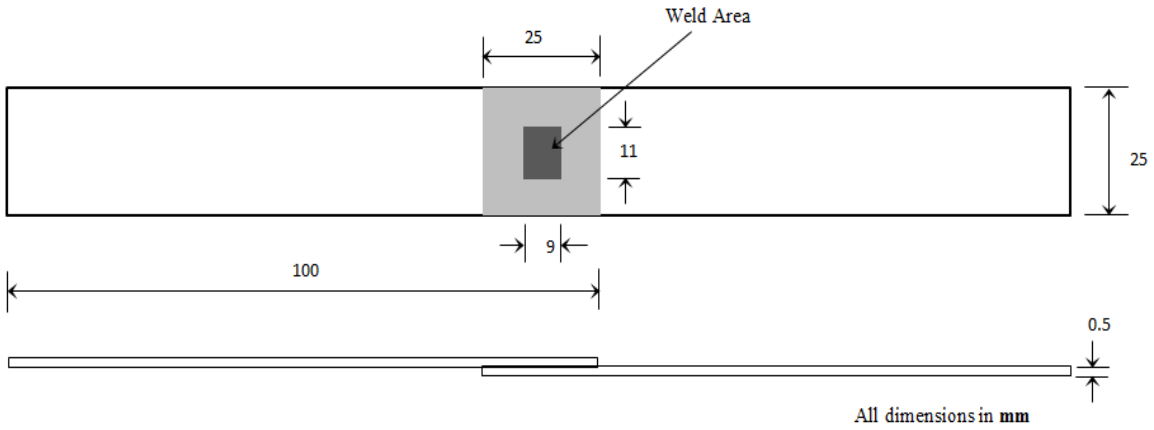

Fig. 5.1 ASTM Standard (D1002-01) specimen

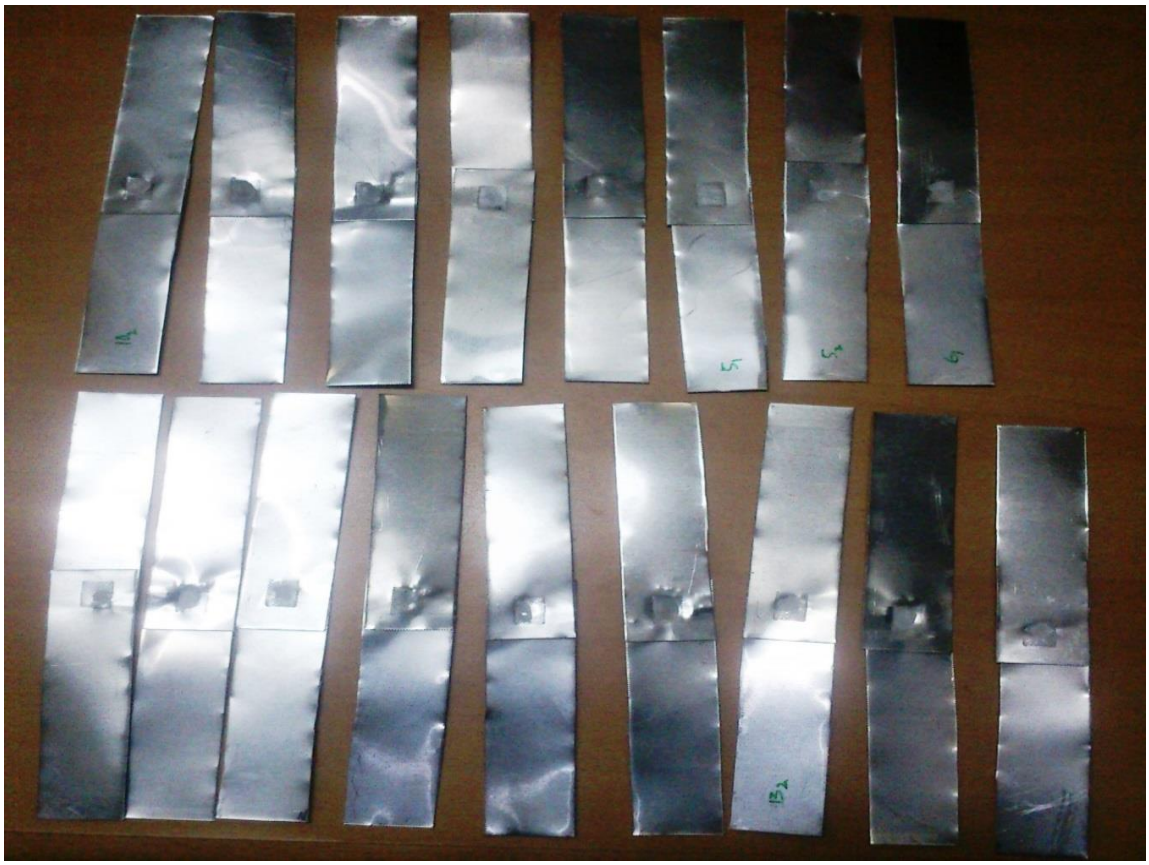

Fig. 5.2 ultrasonically welded specimens

Table 5.2 Experimental table

Exp. no	Pressure	Amplitude	Weld Time	Tensile Strength		
				Trial 1	Trial 2	Avg
1	1.4	21	0.45	74.15	68.06	71.065
2	1.8	21	0.45	90.01	84.38	87.045
3	1.4	27	0.45	83.73	78.89	81.31
4	1.8	27	0.45	83.38	81.97	82.675
5	1.4	24	0.4	83.23	71.77	77.55
6	1.8	24	0.4	86.39	92.58	89.375
7	1.4	24	0.5	88.45	80.64	84.565
8	1.8	24	0.5	92.74	94.17	93.21
9	1.6	21	0.4	86.79	80.31	83.195
10	1.6	27	0.4	74.73	86.55	80.64
11	1.6	21	0.5	90.21	79.56	84.885
12	1.6	27	0.5	85.19	79.74	82.465
13	1.6	24	0.45	87.91	86.73	87.32
14	1.6	24	0.45	87.82	81.4	84.61
15	1.6	24	0.45	86.45	85.9	86.52
16	1.6	24	0.45	87.21	80.93	84.52
17	1.6	24	0.45	86.44	84.51	85.67

The tensile strength of the joint is measured in a Computerized Tensile testing Machine with a constant cross head displacementt of 5 mm/min. It was observed that, a ductile fracture occurs at the periphery of the weld except a few specimens which have poor weld quality. Some of the fractured specimens are shown in Fig. 5.3.

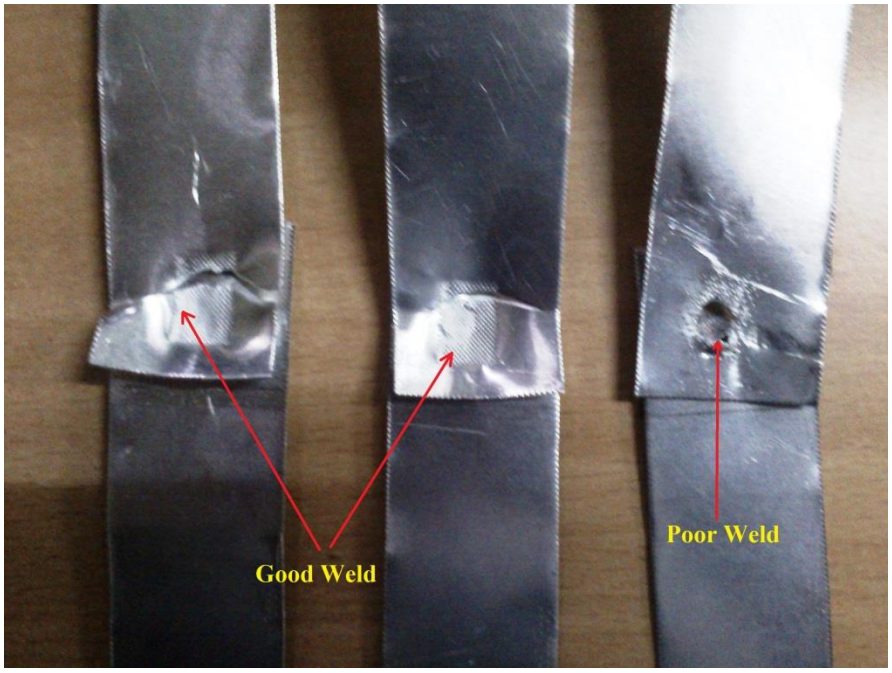

Fig. 5.3 Fractured specimens

5.1.2 Result and Discussion

An extensive analysis is carried out for both the trails values and the average value and it was found out that the average of the response gives the optimum result. The analysis is carried out in popular Design Experts® software. Table 4 shows the analysis of variance (ANOVA) table for tensile strength of the joint. Process variables like A, B, C, B^2 and A*B are significantly affects the model. After eliminating the insignificant process variables those are having a p-value more than 0.05, it was observed that the value of Predicted R-Squared 0.8068 is in reasonable agreement with the value of Adjusted R-Squared 0.8966 which advocates that the variation in the observed value can be explained by the chosen model satisfactorily.

Table 5.3 ANOVA for Tensile strength

Source	Sum of Squares	df	Mean Square	F Value	p-value Prob > F	
Model	345.17	8	43.15	11.41	0.0012	significant
A-Pressure	178.27	1	178.27	47.16	0.0001	
B-Amplitude	0.33	1	0.33	0.075	0.7914	
C-weld time	25.99	1	25.99	6.88	0.0306	
A*B	53.77	1	53.77	14.22	0.0055	
B*C	9.025*E-3	1	9.025*E-3	2.089*E-3	0.9648	
A*C	2.53	1	2.53	0.67	0.4372	
A^2	3.69	1	3.69	0.98	0.3519	
B^2	72.49	1	72.49	19.17	0.0024	
C^2	9.34	1	9.34	2.47	0.1546	
Residual	30.24	8	3.78			
Lack of Fit	20.99	4	5.25	2.27	0.2236	not significant
Pure Error	9.26	4	2.31			
Core Total	375.42	16				

Fig. 5.4 shows the surface plot of tensile strength with pressure and amplitude. It illustrates that with the increase in pressure tensile strength increases as surface asperities come closer which helps the Vander Waal forces act better which leads to better bonding. With the increase in amplitude the strength also increases but after a certain level it slightly decreases as the heat energy is directly proportional to the square of the amplitude. The relation between amplitude and heat energy [18] is given below:

$$Q_{avg} = \frac{f \times \xi_0^{\,2} \times E''}{2} \tag{5.2}$$

where:

Q_{avg} = Heating rate

f = frequency

ξ_0 = applied strain (proportional to amplitude)

E'' = Complex loss modulus of the material

Hence, a little increase in amplitude causes a substantial increase in the heat and material in the deformation zone gets softer which sometimes leads to the joining of the parts with the anvil or sonotrode results in improper welding. Fig. 5.5 and Fig. 5.6 shows the surface plot of tensile strength with welding time and pressure and tensile strength with welding time and amplitude, it can be seen that with increase in welding time and pressure strength increases, this is because as weld time increase it gives sufficient time for scrubbing action and disrupt the contaminants results in better weld. The developed regression equation for maximizing tensile strength of the joint in terms of coded form is given as below:

Tensile strength = +85.62 + 4.72*A + 2.2*B + 1.80*C - 3.67*A*B

$$- 0.80*A*C - 0.94*A^2 - 4.15*B^2 + 1.49*C^2 \quad (5.3)$$

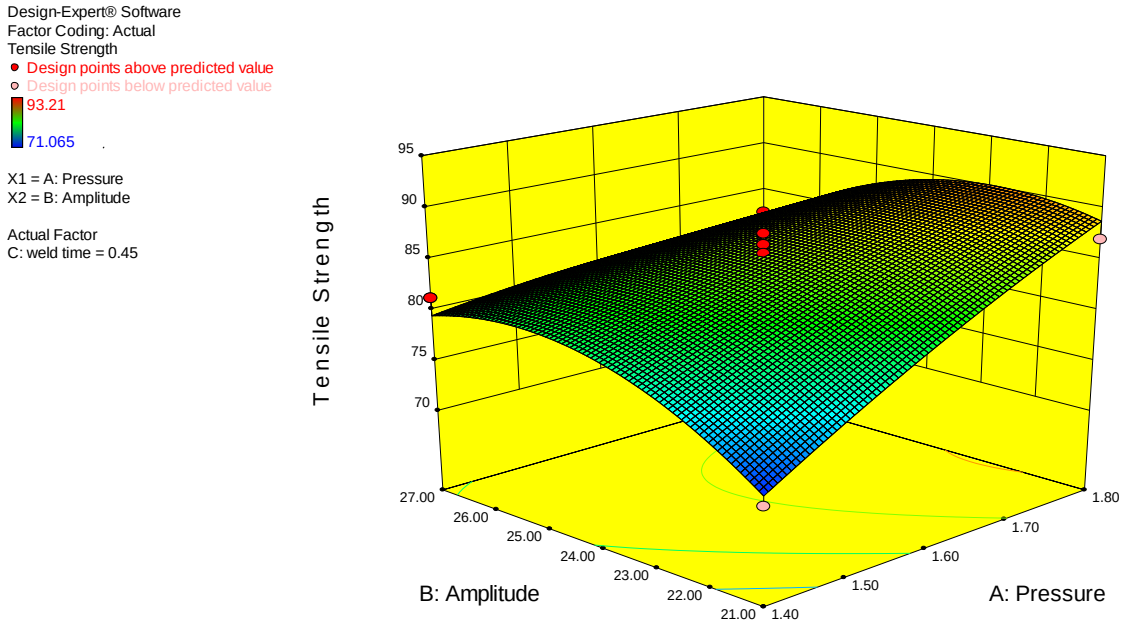

Fig. 5.4 Surface plot of Tensile strength with Amplitude and Pressure

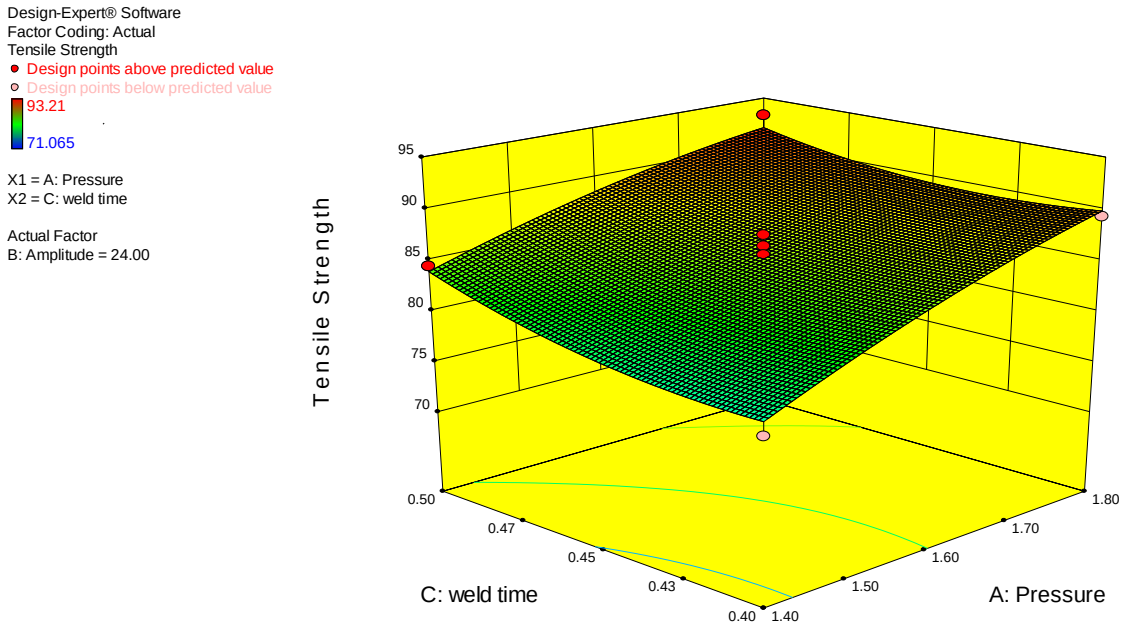

Fig. 5.5 Surface plot of tensile strength with Weld time and Pressure

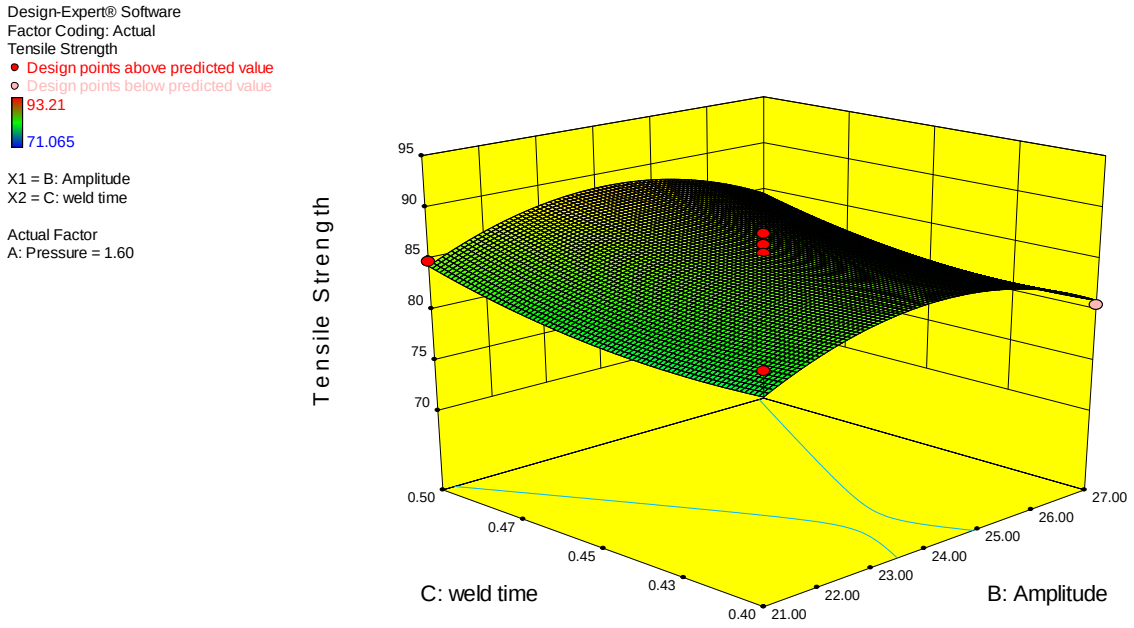

Fig. 5.6 Surface plot of tensile strength with Weld time and Amplitude

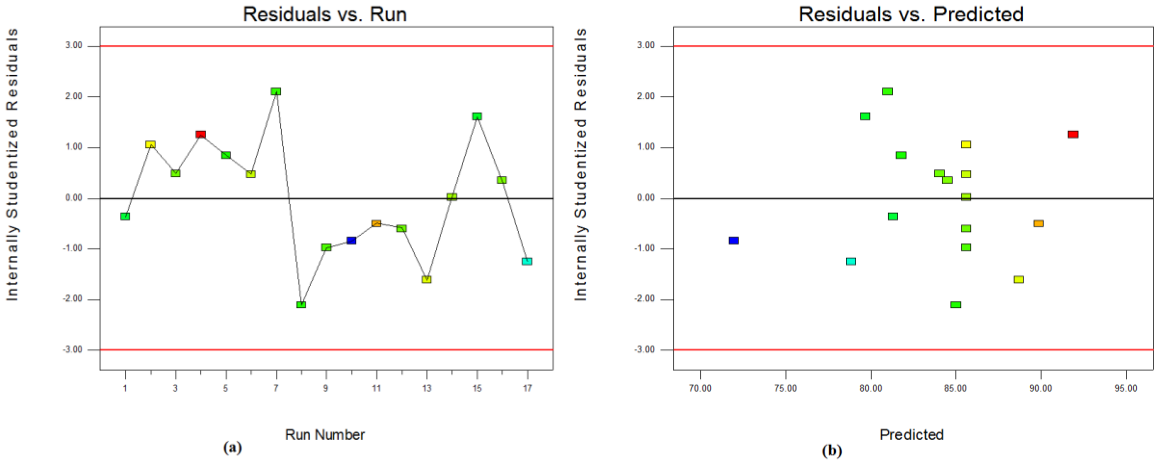

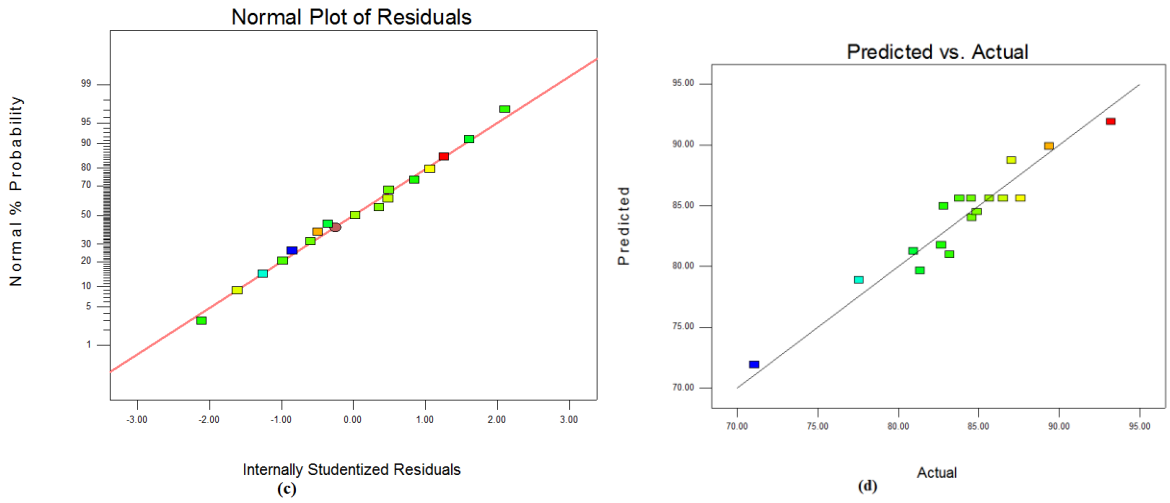

Fig. 5.7 Residual plots for Tensile strengths **(a)** Residuals vs. Run, **(b)** Residuals vs. Predicted, **(c)** Normal plot of residuals, **(d)** Predicted vs Actual

Fig. 5.7 shows the residual plots for tensile strength of the joint. The residuals versus experimental run plot indicate that the runs are evenly scattered around the mean line, this helps in checking for the hidden variables that may influence the response during welding. The residual versus predicted graph shows a random scattering of the values, it checks for constant variance. In the normal plot, the runs are arranged in a straight line which indicates that the residuals are following a normal distribution. The plot between predicted values versus actual value of responses indicates that the values are very close to each other and distributed near the man line.

5.2 Optimization using desirability function

The method was introduced by Derringer and Suich [19]. In this method, the individual responses are altered into a corresponding desirability value and the range of desirability value varies between zero to one. When the value of the response is at its target value, which is the most desired place, then the desirability value is assigned to one. If the value of response is

outside recommended tolerance range which is not desired, then its desirability value is assumed as zero.

In this study higher-the-better criterion is chosen for the tensile strength of the joint. The individual desirability value for this criterion can be calculated by the formula given below:

$$If \quad \hat{y} \le y_{\min}, \qquad d_i = 0 \tag{5.4}$$

$$If \quad y_{\min} \le \hat{y} \le y_{\max}, \qquad d_i = \left(\frac{\hat{y} - y_{\min}}{y_{\max} - y_{\min}} \right)^r \tag{5.5}$$

$$If \quad \hat{y} \ge y_{\max}, \qquad d_i = 1 \tag{5.6}$$

Here $\hat{y}$ represents the value of responses, $y_{\min}$ represents the lower acceptable limit of $\hat{y}$, $y_{\max}$ represents the upper acceptable limit of $\hat{y}$ and r represents desirability function index, which needs to assign formerly as per the consideration of optimization solver. So when the equivalent response is estimated to be nearer to the target, then the function index is set to a higher value.

In this study, $y_{\max}$ is taken as the highest observed value of the response 93.21 MPa and $y_{\min}$ is taken as the lowest observed value of the response 71.065 MPa. The calculated value of process variables and the response is tabulated in Table 5.4 as per the descending order of the calculated desirability value. It was observed that the optimal parameter setting for tensile strength of the joint is pressure 1.8 bar, amplitude 22.75 µm, weld time 0.5 sec. The calculated value of tensile strength of the joint at optimal parameter setting is 92.6065 MPa having a desirability value of 0.973.

Table 5.4 Desirability Table

Number	Pressure	Amplitude	weld time	Tensile Strength	Desirability
1	1.80	22.75	0.50	92.6065	0.973
2	1.80	22.80	0.50	92.6048	0.973
3	1.80	22.70	0.50	92.6045	0.973
4	1.80	22.73	0.50	92.5958	0.972
5	1.80	22.77	0.50	92.5439	0.970
6	1.80	23.13	0.50	92.51	0.968
7	1.80	23.22	0.50	92.4876	0.967
8	1.80	23.06	0.50	92.4789	0.967
9	1.80	23.35	0.50	92.4511	0.966
10	1.80	22.68	0.50	92.4221	0.964
11	1.78	22.41	0.50	92.2718	0.958
12	1.80	23.55	0.40	90.6312	0.884
13	1.80	22.73	0.40	90.6306	0.884
14	1.80	23.73	0.40	90.6252	0.883
15	1.80	24.06	0.40	90.6217	0.883
16	1.80	22.11	0.40	90.6074	0.882
17	1.80	22.73	0.40	90.4968	0.877
18	1.80	22.59	0.40	90.4172	0.874
19	1.80	22.68	0.41	90.4079	0.873
20	1.80	22.72	0.41	90.3949	0.873
21	1.80	24.29	0.41	90.3081	0.869
22	1.80	22.60	0.41	90.3073	0.869
23	1.80	21.97	0.45	90.058	0.858
24	1.80	22.69	0.42	90.0044	0.855
25	1.80	22.75	0.43	89.9779	0.854

Fig. 5.8 shows the surface plot for desirability with amplitude and pressure, it can be seen that the maximum desirability value reached at pressure of 1.8 bar and amplitude of 22.75 µm.

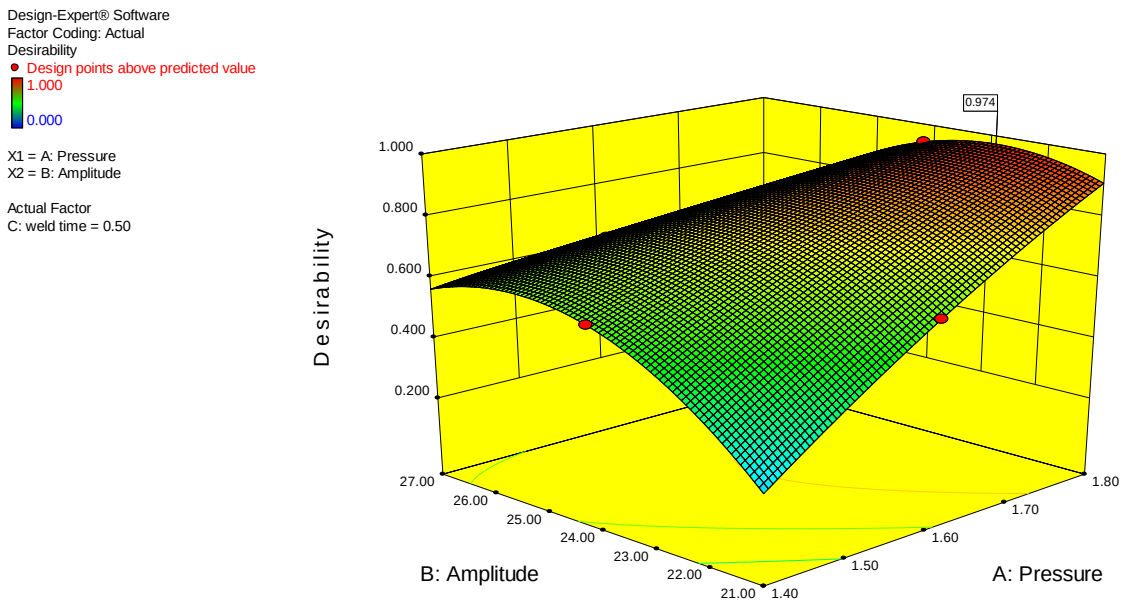

Fig. 5.8 Surface plot for Desirability with Amplitude and Pressure

5.3 Validating the FE model for Temperature Distribution

The temperature at the weld interface is measured during welding with the help of a data acquisition system. The data acquisition system consists of a K-type thermocouple (sensor), a DAQ card, a computer with analyzing software. The thermocouple is capable of measuring a temperature range from -180 ^{0}C to +1260 ^{0}C. Fig. 5.9 shows, the set up for ultrasonic metal welding with temperature measurement attachment.

Fig. 5.9 Experimental set up with temperature measurement attachment

The experiments were conducted at the optimum parameter setting which is evaluated in next chapter. The parameters were set as pressure of 1.8 bar, amplitude at 80% (37.08 μ), and weld time at 0.5 sec. The experiment at same level of parameter is repeated for 3 times and the maximum value of temperature observed is 176.223 ^{0}C with comparing to the model result of maximum temperature 182.069 ^{0}C which was generated in stepped sonotrode shape, a relative error of 3.32% observed. The data gathered from the software is listed in Table 5.5. A graph is plotted for temperature against time in Fig. 5.10.

Table 5.5 Temperature readings with time from lab view software

Si. No.	Temperature (^{0}C)		
	Trial 1	Trial 2	Trial 3
1	29.759544	29.309207	30.524261
2	30.517624	29.333454	30.495402
3	30.358214	29.356395	30.470985
4	30.857415	39.738548	30.413762
5	**176.22367**	**154.31596**	**174.81667**
6	145.17256	123.44487	147.25466
7	91.280436	98.276223	97.756236
8	83.521031	81.943958	85.685131
9	77.393324	63.612485	76.798424
10	73.239116	55.117937	71.836616
11	68.400442	47.973039	68.592462
12	65.860792	42.293895	62.860792
13	63.071146	39.059449	61.071146
14	60.522932	36.584705	57.522932
15	57.650652	36.215455	55.650652
16	55.130103	34.882099	53.130503
17	53.395178	33.268054	51.395178
18	51.252142	32.494824	50.394752
19	49.475485	31.692761	49.632425
20	46.258419	31.293433	47.788949
21	45.413527	30.882567	46.279405
22	44.125496	30.563878	45.294345
23	43.985753	30.403711	44.297961
24	42.751466	31.801993	43.047485
25	41.445751	34.032967	42.070274
26	40.236554	32.636755	41.227193
27	40.449971	32.418425	40.449971

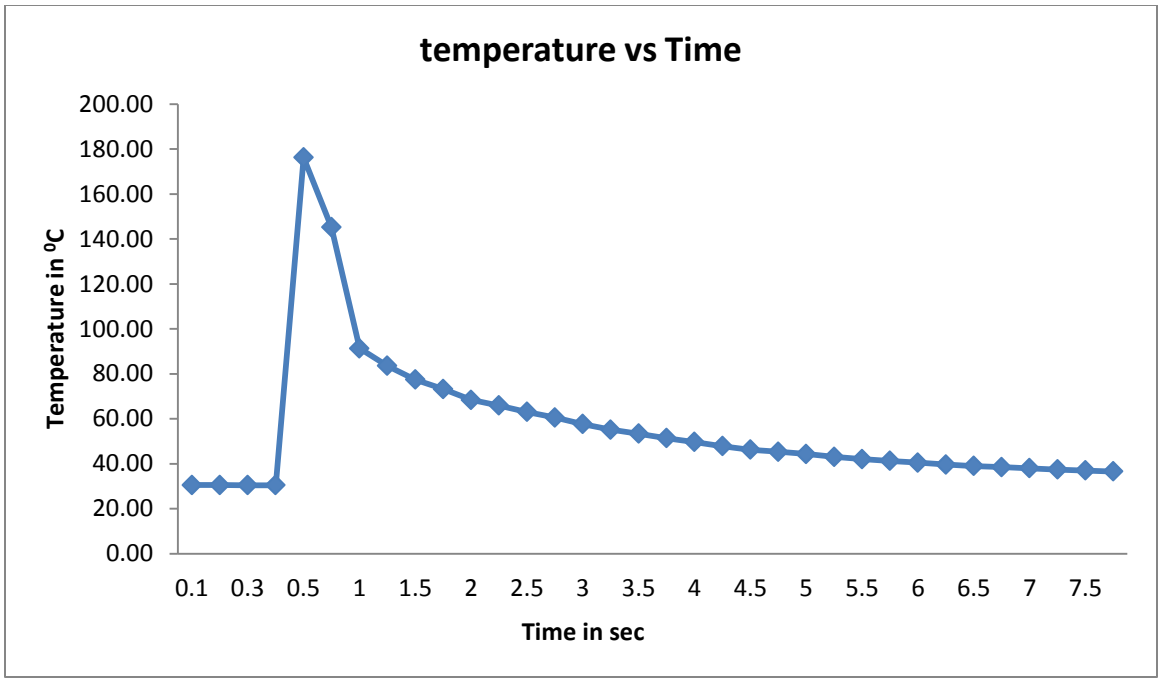

Fig. 5.10 Observed temperature variation with time

5.4 Summary

The above chapter highlights the effect of welding parameters such as pressure, amplitude and weld time on the output response tensile strength of the joint. It was found that the pressure and weld time with interaction between pressure and amplitude were proves to be significant parameters. From the desirability function the optimum parameter setting is obtained as pressure 1.8 bar, amplitude 22.75 µm, weld time 0.5 sec with a desirability value of 0.974. The temperature generation from the FE model is validated by conducting experiment and found out as 176.22 ^{0}C, with a relative error of 3.32%.

CHAPTER 6

CONCLUSIONS

6.1 Summary of the findings

After carrying out a systematic study the following extrapolation can be summarized:

1. An FEM based analysis is done for ultrasonic welding by taking Aluminium as workpiece material and mild steel as sonotrode and anvil material. The model can predict the temperature and stress distribution with different shape of the sonotrode.
2. It can be also understood from the study that the temperature distribution at the work piece is more as compared to the sonotrode and anvil as the thermal conductivity of Aluminum is more as compared to steel and thermal load is applied at the center of the weld.
3. If we compare between different sonotrode shapes then we can see that the temperature generated by stepped shape 182.069^{0}C is maximum as compared to exponential and stepped shape. Similarly, stress generated due to clamping force for the stepped shape 0.627×10^{7} N/m^{2} is maximum.
4. The proposed RSM model gives the importance of the process variables such as pressure, amplitude, and weld time on the tensile strength of the joint.
5. From the desirability function the optimum parameter setting is obtained as pressure 1.8 bar, amplitude 22.75 μm, weld time 0.5 sec with a desirability value of 0.974.
6. The temperature generation from the FE model is validated by conducting experiment and found out as 176.22 ^{0}C, with a relative error of 3.32%.
7. The research work offers an effective guideline to select optimum parameter settings for achieving desired tensile strength.

6.2 Recommendation and Future scope

From the current work it was found out that the conical shape generates minimum value of temperature and stress, so the shape of the tool is recommended when a welding required for soft and thin material. Whereas stepped shape sonotrode is recommended for relatively thick material. For the joining of 0.5 mm Aluminium foil in 3000 W machine, it is recommended that the value of amplitude should be less than 22 μm.

The present research work is carried out for Aluminium as workpiece material and mild steel as sonotrode and anvil material. Still there is a vast area to explore for this novel welding process. Hence, future work can carried out in the following direction:

1. Ultrasonic welding of dissimilar materials with suitable experimental design and parameter setting.
2. Effect of shape of the anvil on the welding process.

References

1. Elangovan, S., Semeer, S., and Prakasan, K. (2009). Temperature and stress distribution in ultrasonic metal welding—An FEA-based study. Journal of materials processing technology, 209(3), 1143-1150.

2. Siddiq, A., and Ghassemieh, E. (2008). Thermomechanical analyses of ultrasonic welding process using thermal and acoustic softening effects. Mechanics of Materials, 40(12), 982-1000.

3. Konchakova, N., Balle, F., Barth, F. J., Mueller, R., Eifler, D., and Steinmann, P. (2010). Finite element analysis of an inelastic interface in ultrasonic welded metal/fibre-reinforced polymer joints. Computational Materials Science, 50(1), 184-190.

4. Levy, A., Le Corre, S., Chevaugeon, N., and Poitou, A. (2011). A level set based approach for the finite element simulation of a forming process involving multiphysics coupling: Ultrasonic welding of thermoplastic composites. European Journal of Mechanics-A/Solids, 30(4), 501-509.

5. De Vries, E. (2004). Mechanics and mechanisms of ultrasonic metal welding(Doctoral dissertation, The Ohio State University).

6. Amin, S. G., Ahmed, M. H. M., and Youssef, H. A. (1995). Computer-aided design of acoustic horns for ultrasonic machining using finite-element analysis. Journal of Materials Processing Technology, 55(3), 254-260.

7. Pandya Bhavik, Patel Saral, and Patel Viral (2014). Effect of horn (sonotrode) profile on weld strength of HDPE plastic by using ultrasonic welding. International Journal for Technological Research and Engineering, 2(4), 2347-4718

8. Zhang, C. Q., Robson, J. D., Ciuca, O., and Prangnell, P. B. (2014). Microstructural characterization and mechanical properties of high power ultrasonic spot welded aluminum alloy AA6111–TiAl6V4 dissimilar joints. Materials Characterization, 97, 83-91.

9. Villegas, I. F. (2014). Strength development versus process data in ultrasonic welding of thermoplastic composites with flat energy directors and its application to the definition of optimum processing parameters. Composites Part A: Applied Science and Manufacturing, 65, 27-37.

10. Panteli, A., Chen, Y. C., Strong, D., Zhang, X., and Prangnell, P. B. (2012). Optimization of aluminium-to-magnesium ultrasonic spot welding. Journal of Minerals, Metals and materials, 64(3), 414-420.

11. Sooriyamoorthy, E., Henry, S. P. J., and Kalakkath, P. (2011). Experimental studies on optimization of process parameters and finite element analysis of temperature and stress distribution on joining of Al–Al and Al–Al2O3 using ultrasonic welding. The International Journal of Advanced Manufacturing Technology, 55(5-8), 631-640.

12. Liu, S. J., Lin, W. F., Chang, B. C., Wu, G. M., and Hung, S. W. (1999). Optimizing the joint strength of ultrasonically welded thermoplastics. Advances in Polymer Technology, 18(2), 125-135.

13. Wijk, H., Luiten, G. A., Engen, P. G., and Nonhof, C. J. (1996). Process optimization of ultrasonic welding. Polymer Engineering and Science, 36(9), 1165-1176.

14. Elangovan, S., Venkateshwaran, S., and Prakasan, K. (2012). Experimental Investigations on Optimization of Ultrasonic Welding Parameters for Copper to Brass Joints Using Response Surface Method and Genetic Algorithm. International Journal of Advanced Engineering Research and Studies, 1(3), 1-6..

15. Harras, B., Cole, K. C., and Vu-Khanh, T. (1996). Optimization of the ultrasonic welding of PEEK-carbon composites. Journal of reinforced plastics and composites, 15(2), 174-182.

16. Kim, T. H., Yum, J., Hu, S. J., Spicer, J. P., and Abell, J. A. (2011). Process robustness of single lap ultrasonic welding of thin, dissimilar materials. CIRP Annals-Manufacturing Technology, 60(1), 17-20.

17. ASTM International Codes, "Standard Test Method for Apparent Shear Strength of Single-Lap-Joint Adhesively Bonded Metal Specimens by Tension Loading (Metal-to-Metal)," ASTM International, Vol.01, 2005, pp. 52-55.

18. Kirkland TR (2001). The implications of the fundamental formulas for frequency selection in ultrasonic plastics welding. In: 31st annual symposium of Ultrasonic Industry Association Atlanta, Georgia, USA.

19. Derringer, G. and Suich, R. (1980) "Simultaneous Optimization of Several Response Variables". Journal of Quality Technology 12, pp. 214-219.

List of Publications

Manas Ranjan Panda, S. S. Mahapatra, Chinmaya P. Mohanty, "**Parametric Investigation of Friction Stir Welding on AA6061 using Taguchi Technique**". Materials Today Journal, Elsevier (accepted).